2008

Phenotypic characterization of canine cranial cruciate ligament associated synoviocytes

Sunil C. Vasanjee
Louisiana State University and Agricultural and Mechanical College, vasanjee@vetmed.lsu.edu

PHENOTYPIC CHARACTERIZATION OF CANINE CRANIAL CRUCIATE LIGAMENT ASSOCIATED SYNOVIOCYTES

A Thesis

Submitted to the Graduate Faculty of the
Louisiana State University and
Agricultural and Mechanical College
in partial fulfillment of the
requirements for the degree of
Master of Science

in

The Interdepartmental Program in
Veterinary Medical Sciences

by
Sunil C. Vasanjee
BVSc, University of Zimbabwe, 2000
May 2008

DEDICATION

To Soheeni for helping me along the way

ACKNOWLEDGEMENTS

This project would not have been possible without the tremendous support of many individuals. I would like to thank Dr Gimble, Dr Hosgood, and Dr Lopez for being on my committee and for guiding me through the project.

I would also like to thank Sandra Robinson and Nakia Spencer from the Laboratory for Equine and Comparative Orthopedic Research Laboratory who dedicated many hours helping with various aspects of the project.

Finally, I appreciate the technical assistance provided by Dr William Henk, Dr Daniel Paulsen, Dr Inder Sehgal, Julie Millard, Olga Borksenious, Kyle Waite, and Greg McCormick.

TABLE OF CONTENTS

LIST OF TABLES

LIST OF FIGURES

ABSTRACT

Identification of synoviocytes surrounding the canine cranial cruciate ligament (CrCL) has not been investigated.

Objectives

1) Develop and validate a technique to identify and quantify normal canine CrCL associated synoviocytes.
2) Compare synoviocyte phenotype proportions surrounding normal and abnormal canine CrCLs

Design

In vitro experimental

Animals

Cranial cruciate ligaments from 4 intact female and 6 intact adult male mixed-breed dogs (objective 1) and from 8 adult female hound dogs (objective 2)

Methods

Objective 1) Normal CrCLs - CD18 and HSP25 epitopes were colocalized using immunohistochemistry. Sagittal sections were quantified in the proximal, middle, and distal aspects of each section. Western blot, RT-PCR and immunoelectron microscopy was used to confirm the presence of CD18 and HSP25 in the canine CrCL.

Objective 2) Normal, artificially stretched and naturally partially disrupted canine CrCLs - CD18 and HSP25 epitopes were colocalized using fluorescent immunohistochemistry. Sagittal sections were prepared from the central aspect of each CrCL and phenotypes were quantified in the proximal, middle, and distal aspects of each section.

Results

Objective 1) Synoviocyte populations stained positive for CD18 (CD18+) or HSP25 (HSP25+), and a small population of cells stained for both epitopes (DS+). The proportion (mean ± SEM) of HSP25 + synoviocytes (57 ± 7.5 %) was significantly greater than the proportion of CD18 + synoviocytes (27 ± 8.2 %), which was significantly greater than the proportion of DS+ synoviocytes (16 ± 3.5%). Western blot, RT-PCR and immunoelectron microscopy confirmed the presence of CD18 and HSP25 epitopes in the canine CrCL.

Objective 2) The pixel count for HSP25 + synoviocytes (57 ± 7.5 %) was significantly greater than the proportion of CD18 + synoviocytes (27 ± 8.2 %), which was significantly greater than the proportion of DS+ synoviocytes (16 ± 3.5%) in all groups. There was no significant difference in the proportions of each of the phenotypes between CrCLs.

Conclusion

Three synoviocyte phenotypes were identified using immunohistochemical staining. Synoviocyte phenotype proportions did not differ between normal and abnormal CrCLs, however the HSP25+ synoviocytes were the predominant phenotype in all CrCLs.

CHAPTER 1. BACKGROUND AND REVIEW OF THE LITERATURE

1.1 Cranial Cruciate Ligament

1.1.1 Microscopic Anatomy

The cranial cruciate ligament (CrCL) is made up of multiple fibers composed of collagen types I, II, III and IV (Arnoczky 1983). A loose band of connective tissue known as the endotenon surrounds each fascicle (Arnoczky 1983). The individual fascicles are oriented in a spiral fashion around the long axis of the ligament or pass directly between the bony attachments of the ligament (Arnoczky 1983). The fascicles collectively are surrounded by the paratenon, a connective tissue covering (Arnoczky 1983). The CrCL is enveloped by a fold of synovium which divides the joint in a sagittal plane (Arnoczky 1983). Therefore, though the CrCL is intra-articular, it is actually extra-synovial. This synovial membrane resembles a mesentery and is richly endowed with blood vessels that originate primarily from the middle geniculate artery (Arnoczky 1979, Arnoczky 1983).

Figure 1.1 Photomicrograph of a normal canine cranial cruciate ligament. The long arrow represents the synovium, the short arrow represents the collagen fibers, and the arrow head represents the blood vessels within the synovium.

1.1.2 Macroscopic Anatomy

The CrCL originates on the medial aspect of the lateral femoral condyle, traverses diagonally, and attaches on the tibia cranial and lateral to the tibial spine (Arnoczky 1983). The bony attachments do not occur as a single cord, but instead as a collection of individual fibers that fan out over a broad flattened area (Arnoczky 1983). These fibers are divided into a craniomedial band and a caudolateral band (Arnoczky 1983). Both the craniomedial and caudolateral bands function reciprocally during extension and flexion of the stifle such that part of the ligament is taut at any given joint angle (Odensten et al. 1985, Hirokawa et al. 2001). When the stifle is extended both bands are taut.(Odensten et al. 1985, Hirokawa et al. 2001). However when the stifle is flexed, the craniomedial band tightens and the caudolateral band loosens.(Girgis et al. 1975). Also present is an intermediate component, which represents the transition between the craniomedial band and the caudolateral band with fibers in varying degrees of tension.(Girgis et al. 1975).

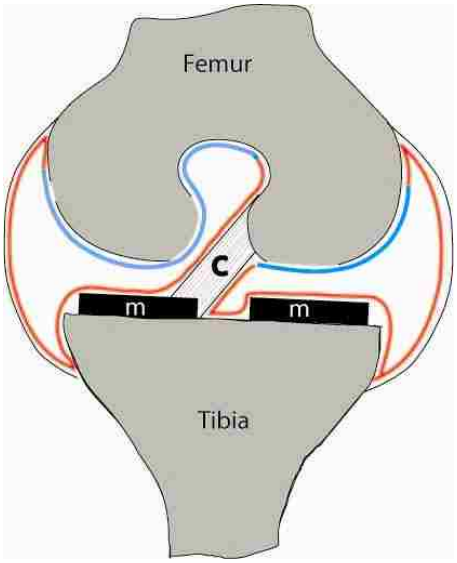

Figure 1.2 Schematic diagram of stifle, CrCL and the synovium. Note how the synovium surrounds the CrCL such that the CrCL does not come into contact with the joint fluid. (C = CrCL, m = meniscus, and red line represents the synovium)

1.1.3 Comparative Anatomy

The CrCL is well conserved across mammalian species both in function and structure. However, differences between species exist. Murray compared CrCLs from multiple species, including human, bovine, ovine, and canine (Murray et al. 2004). She found normal human CrCLs to be similar to canine CrCLs with respect to fibroblast density, smooth muscle actin expression, vascularity, and fibroblastic cell nuclear morphology (Murray et al. 2004). When human CrCLs were compared to bovine CrCLs differences were noted in vascularity and cell morphology (Murray et al. 2004). The bovine CrCLs consisted of fewer spheroid fibroblasts and greater vessel density than human CrCLs (Murray et al. 2004).

1.1.4 Innervation

Innervation of the CrCL is by way of fibers from branches of the tibial nerve (Arnoczky 1983). Four distinct types of articular receptor endings (mechanoreceptors) – Ruffini endings, Pacinian corpuscles, Golgi tendon organ-like endings and free nerve endings have been identified in the human and feline CrCL (Girgis et al. 1975). Mechanoreceptors have also been identified in the feline and human joint capsule, human menisci, feline collateral ligaments, and human infrapatellar fat pad (Halata et al. 1985, Zimny et al. 1988, Sojka et al. 1991, Krauspe et al. 1992). Mechanoreceptors are pressure sensitive corpuscles that send impulses to the brain during stifle motion (Krauspe et al. 1992). The exact role that these receptors play in the CrCL is not known, however, they are thought to play a role in proprioception, pain perception, and the regulation of blood flow (Krauspe et al. 1992). Proprioception has been shown to be deficient in human patients with CrCL rupture and correlations have been seen with reduced proprioception and increased age, low activity level, and cartilage injuries following CrCL rupture (O'Connor et al. 1989, Masayoshi 2004). In addition to affecting proprioception, CrCL rupture has been

shown to affect motor co-ordination on a global level, including head and trunk abnormalities (O'Connor et al. 1989, Masayoshi 2004).

1.1.5 Function

Stability of the stifle joint is achieved through the action of soft tissues including muscles, ligaments, menisci, and the joint capsule (Arnoczky 1977, Arnoczky et al. 1977). The CrCL is the most important stabilizer of the stifle. The function of the CrCL is to prevent cranial displacement of the tibia relative to the femur, prevents hyperextension of the stifle and acts as a restraint against abnormal medial axial rotation during flexion of the stifle (Arnoczky 1977, Arnoczky et al. 1977).

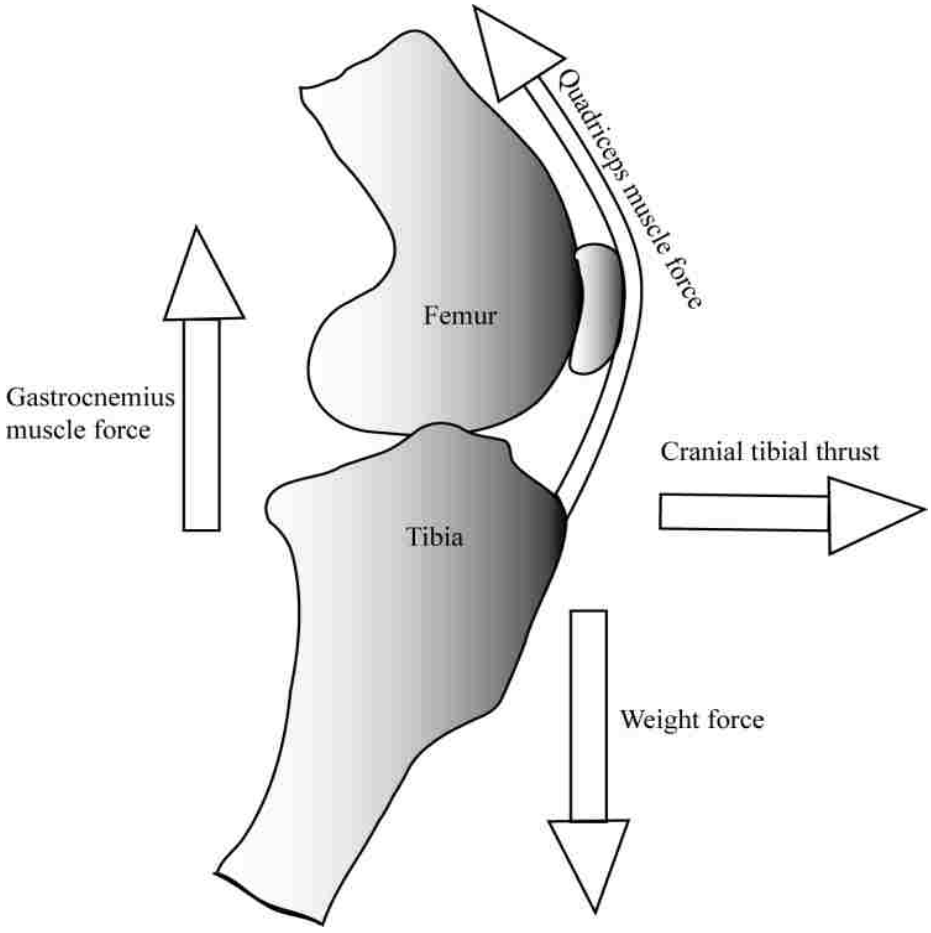

Figure 1.3 Schematic representation of various forces acting on the stifle

1.1.6 Rupture

Rupture of the CrCL is one of the most common causes of hind limb lameness in the dog (Lampman 2003, Powers et al. 2005). A survey carried out in 2003 estimated that dog owners in the USA spend over a billion dollars a year for the treatment of CrCL injury (Wilke et al. 2005). Similarly, in people, billions of dollars are spent each year for treatment of CrCL rupture (Cumps et al. 2007). Disruption of the support mechanism that the CrCL provides alters the joint kinematics, induces joint instability, and contributes to osteoarthritic changes. Rupture of the CrCL is considered multifactorial and is classified as either traumatic or atraumatic. Progressive degeneration of the CrCL is known to lead to rupture of the ligament.

Poteinases such as tartrate-resistant acid phosphatase (TRAP), matrix metalloproteinases (MMPs) and cathepsin K are increased in ruptured CrCLs as compared to normal CrCLs suggesting that these proteins may play a role in the progressive degeneration of the CrCL (Muir et al. 2002). It is not known whether these proteinases are elevated prior to rupture or if they are a consequence of rupture. Tartrate-resistant acid phosphatase has been localized to macrophage-like synoviocytes within the joint capsular synovium suggesting that the synovium may also play a role in CrCL rupture (Muir et al. 2002). Furthermore, cytokine induced expression of modulators of inflammation such as nitric oxides are elevated in ruptured CrCLs leading to premature apoptosis of the CrCL (Murakami et al. 2005, Murakami et al. 2006).

1.1.7 Unilateral and Bilateral Rupture

Though unilateral CrCL rupture is the most common presentation in the dog, up to 37 % of CrCL ruptures are bilateral (Doverspike et al. 1993). Rupture of the contra-lateral CrCL has been reported to occur between ten and twenty two months after diagnosis of the contra-lateral rupture (Doverspike et al. 1993). The pathogenesis behind bilateral CrCL ruptures is not known.

It has been shown that contra lateral limb loading is not increased following transection of the CrCL, so from a mechanical stand point, a CrCL rupture in one stifle should not predispose the contra-lateral CrCL to rupture (O'Connor et al. 1989, Doverspike et al. 1993). Human females have been shown to be at increased risk for bilateral tears (Tifford et al. 2001). Also, an inheritance factor has been suggested in people with bilateral CCL rupture. In one study up to 31% (11/31) human patients with bilateral CrCL rupture had a family history of CrCL rupture (Harner et al. 1994). Inheritance patterns have also been identified in canines (Wilke 2004). Wilke et al detected a recessive mode of inheritance in the Newfoundland breed (Wilke 2004). They however found the inheritance to be of partial penetrance, and therefore not all dogs with the recessive genotype exhibited clinical signs (Wilke 2004).

1.1.8 Healing Potential

Following complete rupture of the human and canine CrCL, the ligament fails to heal and eventually bridge (Murray 2000, Hayashi et al. 2003). The ruptured human CrCL undergoes four distinct phases of tissue repair, which include inflammation, epiligamentous regeneration, proliferation and remodeling (Murray 2000, Hayashi et al. 2003). However, despite the effort to repair itself, a bridging scar does not form (Murray 2000, Hayashi et al. 2003). Proliferation of synovium at the sites of rupture may inhibit formation of the bridging scar. Development of a bridging scar may be further prevented by the expression of myofibroblasts which result in retraction of the CrCL ends (Murray 2000, Hayashi et al. 2003).

Studies have been designed to investigate the healing potential of both partially and completely ruptured CrCLs. Hefti et al reported no regeneration of the CrCL following complete transection in male rabbits and months following complete transection no CrCL remnants remained (Hefti et al. 1991). In contrast, partially ruptured CrCLs were repaired with connective

tissue within 6 weeks (Hefti et al. 1991). Proliferation of fibroblasts appeared to originate from the synovial membrane surrounding the CrCL (Hefti et al. 1991). One year after partial transection the connective tissue resembled normal ligamentous tissue (Hefti et al. 1991). Biomechanical testing of the ligaments revealed progressive strengthening over time with ligamentous failure rates of 88% and 56%, three months and one year after partial transection respectively (Hefti et al. 1991). Naturally occurring disruption of human CrCLs that involves less than 25% of the ligament have been shown to heal (Noyes et al. 1989). Tears involving 50% or 75% of the CrCL progressed to complete rupture 50% and 86% of the time respectively (Noyes et al. 1989). However, magnetic resonance image (MRI) confirmed complete CrCL rupture in an adult human, healed completely within one year (Nawabi et al. 2006). Complete healing of the CrCL was confirmed one year after the injury via arthroscopy (Nawabi et al. 2006).

Manipulation of the intra-articular stifle environment has been carried out in order to stimulate healing of partially ruptured CrCLs.(Kobayashi et al. 1997). Kobayashi et al attached basic fibroblast (bFGF) impregnated beads to partially transected canine CrCL sites (Kobayashi et al. 1997). In vitro, bFGF stimulates growth of mesenchymal cells, induces plasminogen activator, and enhances cell migration (Rifkin et al. 1989). In vivo, bFGF induces neovascularization and subsequent wound repair (Greenhalgh et al. 1990). Kobayashi et al reported a pannus like tissue extending from the synovium as early as one week after the rupture (Kobayashi et al. 1997). At three weeks the defects were completely filled by granulation tissue, and by six weeks the granulation tissue was replaced by ligamentous tissue (Kobayashi et al. 1997). No such healing was seen in the control group in which a non bFGF impregnated bead was implanted at the rupture site (Kobayashi et al. 1997). Despite totally filling the defect, the

ligamentous tissue had an irregular collagen fiber network two years following partial rupture (Kobayashi et al. 1997). No mechanical testing of the ligaments was carried out (Kobayashi et al. 1997). In a canine partial CrCL rupture model, healing of the CrCL had not occurred 6 weeks after creation of the defect (Spindler et al. 2006). However, infusion of a collagen protein rich plasma scaffold into this model stimulated healing of the CrCL histologically and biomechanically (Murray et al. 2006). Bone marrow derived mesenchymal stem cells (MSCs) injected into rabbit stifle joints with artificially created partial CrCL tears has been shown to promote healing of the CrCL, whereas no healing occurred in control joints in which no MSCs were injected (Kanaya et al. 2007).

As has been previously mentioned, retraction and enzymatic degradation of the CrCL stumps is thought to prevent healing of a completely ruptured CrCL (Hayashi et al. 2003). In order to counteract this effect, Demirag et al infused alpha 2 macroglobulin into the stifles of rabbits after experimental transection of the CrCL (Demirag et al. 2004). Alpha 2 macroglobulin is an inhibitor of metalloproteinase enzymes such as collagenases (Demirag et al. 2004). Ten days following infusion, the CrCL stumps retained their brightness, volume, and had not retracted (Demirag et al. 2004). In contrast the CrCL stumps in the control group in which saline was infused were swollen, showed signs of degeneration and had retracted (Demirag et al. 2004). Due to the short duration of the study (ten days), any further effect that the alpha 2 macroglobulin had on the CrCL was not evaluated (Demirag et al. 2004).

1.1.9 Factors Associated With Rupture

Breeds such as the Newfoundland, boxer, Siberian husky, bichon frise, Saint Bernard, rottweiler, Labrador retriever, Neopolitan mastiff, akita, Chesapeke Bay retriever, and the American Staffordshire terrier are at increased risk of CrCL rupture (Duval et al. 1999,

Lampman 2003). The reason why these breeds are more at risk is not known, however a genetic predisposition has been identified in the Newfoundland (Wilke 2004). Size of the CrCL may also contribute to rupture: Biomechanical comparison of the rottweiler and greyound CrCLs revealed that rottweilers CrCLs required only half the load to rupture per unit body mass than did the greyhound CrCLs (Wingfield et al. 2000). Size of the dog may also play a role. Dogs weighing greater than 22Kg had the highest incidence of CrCL rupture than dogs weighting less than 22Kg (Duval et al. 1999).

A narrow intercondylar notch has been shown to be associated with rupture of the CrCL in people and dogs (Anderson et al. 1987, Aiken 1995). The intercondylar notch (ICN) lies between the distal femoral condyles and consists of four structures including the cranial outlet, intercondylar shelf, caudal arch, and caudal outlet. Narrowing of the ICN is usually due to chondrophyte or osteophyte formation associated with degenerative joint disease following rupture of the CrCL (Anderson et al. 1987). However, congenital stenosis of the ICN has been described in people and has been shown to be associated with CrCL rupture (Anderson et al. 1987). Similarly in dogs with naturally occurring CrCL rupture, the ICN width is narrower than in dogs without CrCL rupture (Aiken 1995). It is thought that the CrCL is constricted within the confines of the of the ICN leading to rupture of the CrCL (Anderson et al. 1987, Aiken 1995).

Neutered and spayed dogs have been shown to be at increased risk for CrCL rupture (Duval et al. 1999, Slauterbeck et al. 2004). Compared to male intact dogs, male neutered dogs, and female intact dogs seen for various conditions at a private referral practice, female spayed dogs had the highest incidence of CrCL rupture (5.15%) across size and breed (Slauterbeck et al. 2004). The sexually intact males had the lowest incidence (2.09%) of CrCL rupture (Slauterbeck et al. 2004).

The incidence of human female CrCL tears is three and a half times higher than that of human males (Arendt et al. 1995). Non contact mechanisms are the primary cause of human female CrCL tears (Arendt et al. 1995). Potential risk factors cited for human female CrCL rupture include body movement, muscular strength, shoe surface interface, joint laxity, limb alignment, ICN size, hormonal influence, and ligament size (Arendt et al. 1995).

Dragoo et al recently reported relaxin, a peptide hormone to be associated with ruptured CrCLs in the human female (Dragoo et al. 2003). Relaxin is secreted by the corpus luteum during pregnancy and by the ovaries during the luteal phase (Qin et al. 1997). It facilitates the birth process by causing softening and lengthening of the cervix and the pubic symphysis (Qin et al. 1997).

Relaxin receptors have been immunolocalized to fibroblasts in the CrCL stroma and to cells in the synovial lining and blood vessel walls of the human female CrCL (Bryant-Greenwood et al. 1995, Qin et al. 1997). Its primary effect is via activation of MMP 9, a type IV collagenase (Bryant-Greenwood et al. 1995, Qin et al. 1997). This activation could result in remodeling and weakening of the CrCL by digesting the collagen fibers that make up the CrCL.

Immune mediated disease has also been associated with CrCL disease and rupture. Goldberg et al reported weakening of rabbit CrCLs following experimentally induced immune synovitis and antibodies to collagen I and II and immune complexes have been detected in sera, synovial fluid and synovium of dogs with ruptured CrCLs (Goldberg et al. 1982, Niebauer et al. 1982, Niebauer et al. 1987, Bari et al. 1989, Lawrence et al. 1998, de Rooster et al. 2000). However, these same antibodies and immune complexes have also been detected in the same fluids from dogs with various causes of osteoarthrosis secondary to other pathologic conditions including rheumatoid arthritis, infective arthritis and idiopathic arthritis (Goldberg et al. 1982,

Niebauer et al. 1982, Niebauer et al. 1987, Bari et al. 1989, Lawrence et al. 1998, de Rooster et al. 2000). Therefore it is still unclear whether these antibodies and immune complexes play a role in the primary etiologic mechanism in CrCL rupture, or if they occur secondary to CrCL rupture.

1.2 Biomechanics of the Stifle

1.2.1 Passive Two Dimensional Model

The stifle is a complex condylar synovial joint composed of the femorotibial and femoropatellar joints (Howard 1993). Though the exact biomechanics of the stifle are yet to be established, several models of the stifle have been developed and have evolved over the years. It is important to understand how the biomechanics of the stifle and the function of the CrCL are related. The oldest described model of the stifle was derived by analysis of sagittal sections through the femoral condyles (Arnoczky 1977, Gerber 1983). In this model the stifle is assumed to be a two dimensional, single degree of freedom linkage moving in a frictionless, single plane (Slocum et al. 1993). Since this dictates that the femur and tibia have no forces acting upon them, it is considered a passive force model (Slocum et al. 1993). The CrCL, caudal cruciate ligament (CdCL), tibia, and femur form a four bar hinge mechanism (Goodfellow et al. 1978). This model explains cranial translation of the tibia relative to the femur (cranial drawer), if the CrCL is ruptured (Goodfellow et al. 1978). The discrepant distances between successive points of contact indicate that caudal rolling is accompanied by cranial sliding at a ratio of about two to one (Goodfellow et al. 1978).

Due to the non circular geometry of the femoral condyles and the structure of the ligamentous and muscular constraints, the axis of rotation of the femur relative to the tibia does not remain constant as the stifle is flexed, unlike a simple pivot joint such as the hock joint (Arnoczky 1977). However, at any one instant in time, there is a point on the femur which has

zero velocity with respect to the tibia (Arnoczky 1977). This point varies with the degree of flexion, and is called the instantaneous center of rotation (ICR) (Arnoczky 1977). The ICR is determined by identifying the displacement of two points on the femur as the femur moves from one position to another relative to the tibia (Arnoczky 1977). The lines defined by the displacement are bisected, and the intersection of the perpendicular bisectors represents the ICR (Arnoczky 1977). When the stifle is flexed the ICR is closest to the joint surface which results in slackening of the collateral ligaments and the CrCL (Smith et al. 2003). In extension the ICR is furthest from the articular surfaces resulting in tensing of the collateral ligaments and the CrCL (Smith et al. 2003). This brings the stifle into its most stable position (Smith et al. 2003).

There are several pitfalls in this model. Firstly, it does not take in to account the active forces such as the muscles and gravity acting upon the stifle. Secondly, the ICR theory assumes that the flexion and extension axis lies exactly in the sagittal plane. The flexion-extension axis of the stifle has been shown to be offset from the sagittal by seven degrees (Hollister et al. 1993, Smith et al. 2003). Therefore, this would result in a single, fixed axis and not an ICR (Smith et al. 2003). Secondly, a non fixed axis is less efficient than a fixed axis as a constantly moving axis is inefficient because the moment of inertia is also constantly changing (Smith et al. 2003).

1.2.2 Active Two Dimensional Model

In an attempt to address the deficiencies of the passive model, the active model was derived. It is an expansion of the two dimensional model which also takes into account the effects of muscular and weight bearing forces on the stifle (Slocum et al. 1993). The foundation for the active model is cranial tibial thrust. Cranial tibial thrust is an internally generated force through interaction of the femoral condyles and the tibial plateau (Slocum et al. 1993). Weight bearing and the effect of extensors of the limb (gastrocnemius and quadriceps) results in tibial

compression (Slocum et al. 1993). Because of the slope of the tibial plateau, and because the contact point between the tibia and femur lies cranial to the forces directed through the stifle, tibial compression (during weight bearing or tibial compression test) results in a cranially directed tibial force (Slocum et al. 1993). When the CrCL is ruptured this force results in cranial tibial translation (Slocum et al. 1993).

1.2.3 Three Dimensional Model

With the advent of total stifle arthroplasty, a thorough understanding of stifle kinematics was necessary since inadequate stifle axis reproduction has been shown to cause loosening and accelerated wear of the stifle prosthesis (Walker et al. 1972). With the aim of improving prosthetic design, MRI, radiostereometry, and computed tomography have been used to build a 3 – dimensional model of stifle motion (Kurosawa et al. 1985, Blankevoort et al. 1996, Siu et al. 1996, Sathasivam et al. 1997, Iwaki et al. 2000, Smith et al. 2003).

Three independent axes of motion within a novel human stifle model have been described (Hollister et al. 1993, Iwaki et al. 2000). Between 15 and 150 degrees of stifle flexion, the caudal condylar axis is effective and it is offset from the sagital plane by 7 degrees (Hollister et al. 1993, Hollander et al. 2004). As the stifle approaches extension, the axis shifts from the caudal condylar axis to the to the cranial condylar axis (Hollister et al. 1993, Hollander et al. 2004). The third axis is the longitudinal axis of rotation (Hollister et al. 1993, Hollander et al. 2004).

The medial condyle is shorter and wider than the lateral condyle resulting in an axis of rotation during flexion and extension (Hollister et al. 1993). The exact location of the axis of rotation is dependent on the asymmetry of the tibial plateau (Hollister et al. 1993). Since the medial tibial plateau is concave and deepened by the medial meniscus, and the lateral tibial

plateau is saddle shaped, the axis of longitudinal rotation of the stifle is centered through the medial side of the stifle (Iwaki et al. 2000).

1.3 The Synovium

The CrCL is intimately associated with the synovial membrane surrounding it (Arnoczky 1983). While the synovial membrane is normally a supportive structure, playing a role in synovial fluid generation, maintenance and joint immunity, cells within the synovium play an active role in some arthritides, primarily through generation of inflammatory mediators (Bari et al. 1989). Three synoviocyte phenotypes have been identified in the intimal layer of human joint capsular synovium; macrophage like (type A), fibroblast like (type B), and an intermediate type (Stevens et al. 1990, Wilkinson et al. 1992).

Type B synoviocytes have been conclusively identified in human stifle joint capsule with monoclonal antibody 67 (CD55) staining and uridine diphosphoglucose dehydrogenase (UDPGD) activity (Stevens et al. 1990, Wilkinson et al. 1992). In the horse, joint capsular type B synoviocytes have been identified using the neuronal marker PGP 9.5 (Kitamura et al. 1999). Type A synoviocytes have been positively identified in the human stifle joint capsule with CD68 antibody and non specific esterase (NSE) activity (Stevens et al. 1990, Wilkinson et al. 1992).

Though joint capsular synovial cells resembling macrophages and fibroblasts have been identified in a number of species, published reports differ on their origin/behavior. One report indicates that porcine joint capsular synoviocytes belong to a single cell line originating from the mononuclear phagocyte system that can differentiate into either type A or type B cells (Barratt et al. 1977). Another report indicates mouse type A cells are derived from bone marrow (Edwards et al. 1982). Maekawa et al used light and electron microscopy to evaluate the synoviocytes within rat synovium associated with the infrapatellar fat pad (Maekawa et al. 1996). They

reported seeing type A and type B cells (Maekawa et al. 1996). The type A cells contained lysosomes and the type B produced fibronectin and laminin (Maekawa et al. 1996). Interestingly they were able to identify transformation of type B cells to type A cells (Maekawa et al. 1996). This study suggests that the type B cells are a type of stem cell capable of differentiation into different phenotypes dependent on the condition of the CrCL.

1.4 Identification and Validation of Synoviocyte Phenotypes

1.4.1 Immunohistochemistry

An antigen-antibody complex is the basis for immunohistochemistry. A labeled antibody directly or indirectly binds to an antigen of interest within a section of tissue. The label may be a fluorescent dye, enzyme, radioactive element or colloidal gold. Frozen or formalin fixed samples may be used for immunohistochemistry. The advantage of formalin fixed samples over frozen is that tissue architecture and cell morphology is maintained. Frozen sections are not commonly used because they are difficult to section which may compromise tissue architecture and cell morphology, have poor resolution at higher magnifications, and special storage is needed.

The main advantage of frozen sections over formalin sections is that antigen retrieval is not required. Formalin fixation causes protein cross linking over the antigenic sites thereby preventing antibody access to the antigen. Following fixation in formalin for at least 24 hours, the tissue is embedded in paraffin wax. Embedding in paraffin may alter or even destroy the antigens. Once embedded in paraffin wax, sections ranging in thickness from 5-7 micrometers are prepared using a microtome. Immediately following sectioning the sections are immersed in warm water. This helps smooth the section. After a few minutes the sections are transferred to glass slides. The slides are then dried on a hot plate at just above the melting temperature of the paraffin wax.

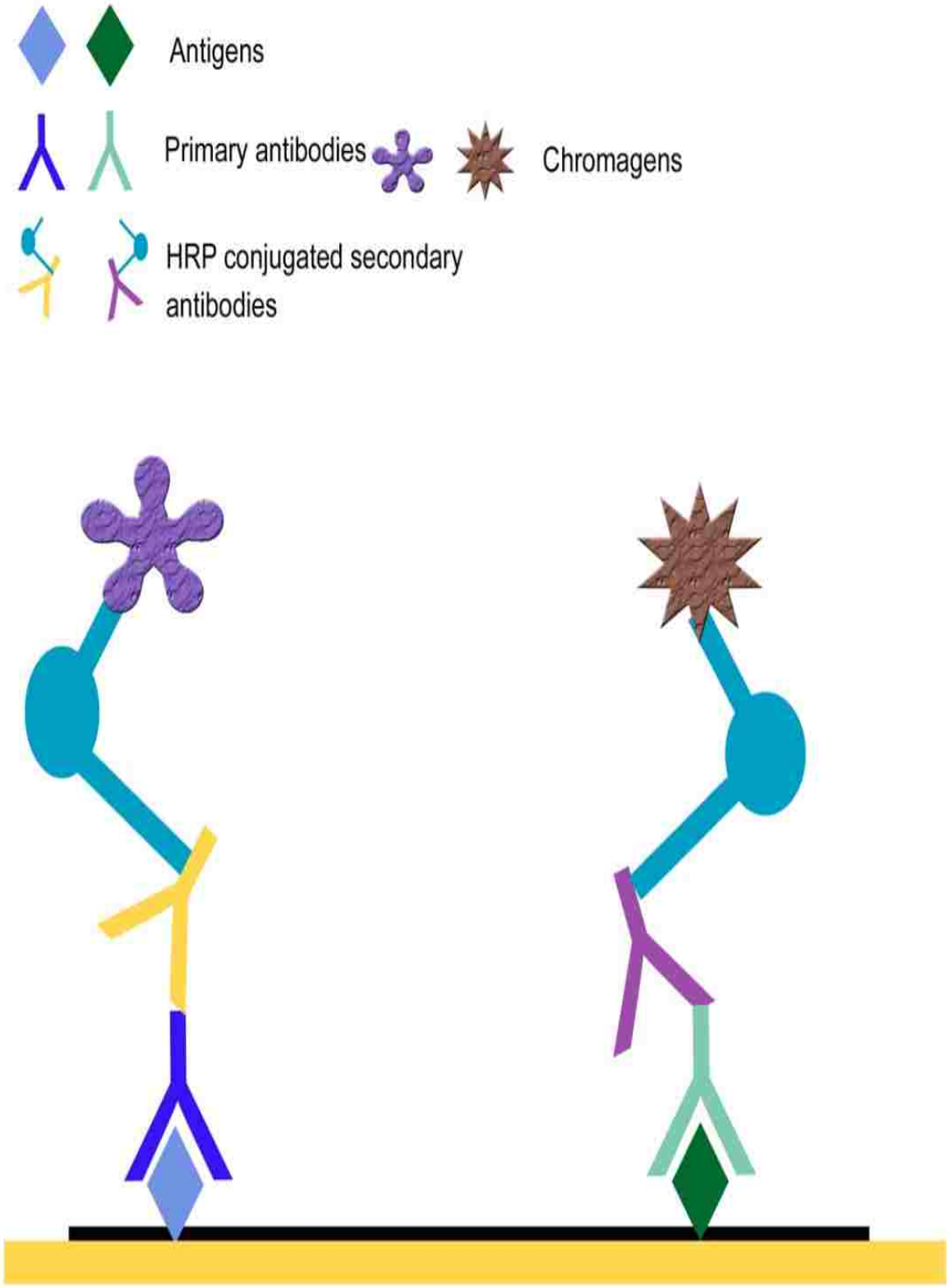

Figure 1.4 Schematic Representation of Double Immunolabelling

Prior to immunohistochemical staining, the paraffin wax must be removed. The sections are immersed in xylene which dissolves the paraffin wax. In order to attain their original architecture and morphology, the sections are hydrated by immersing in alcohol ranging in concentration from 100% to 70% and finally in water. Dependent on the antigen, antigen retrieval may or may not be required. Heat or protein digestion or both are used for antigen retrieval.

When heat is used, sections are immersed in a buffer solution such as citrate buffer, which is then exposed to a heat source such as a microwave oven, pressure cooker, steamer, or hot water bath. When protein digestion is used, the sections are immersed in an enzyme such as trypsin, proteinase K, and pepsin.

Before incubation of the sections with the antibody, the section must be blocked. In addition to binding to the specific antigen, the antibody may also bind to non specific sites. Binding at these non specific sites is not through an antigen-antibody complex, but through electrostatic forces. If the antibodies is allowed to bind to these non specific sites background staining will result. Background staining will affect the quality of the slides and may make interpretation difficult. In order to prevent this background staining the sections are incubated in normal serum which blocks the non specific sites.

The antibody that binds directly to the antigen is referred to as the primary antibody. The primary antibody may have a label attached to it. Instead of using just one antibody, two antibodies may be used. The second antibody that is specific to and that will bind to the primary antibody is referred to as the secondary antibody. In this case the secondary antibody is labeled and this technique is referred to as indirect immunohistochemistry. The secondary antibody must be against the IgG of the animal species in which the primary antibody has been raised. Antibody

labels for light microscopy include chromogens such as DAB and fluorescent dyes such as FITC, rhodamine or Texas red.

Since endogenous peroxidase and phosphates are present in many tissues, in order to minimize the amount of background, the section must be blocked with hydrogen peroxide in the case of antibodies labeled with peroxidase, or with levamisole in the case of antibodies labeled with phosphatase. The indirect method is most commonly used as it is more sensitive due to signal amplification through several secondary antibody reactions with different antigenic sites on the primary antibody. For antibodies attached to an enzyme, in order to visualize the antigen-antibody reaction, the tissue is incubated in a chromogenic substrate that will develop a color (chromogen) when exposed to the enzyme attached to the secondary antibody. The chromogen can then be seen with bright field light microscopy. For antibodies attached to a fluorescent dye, the reaction is seen with a fluorescent microscope.

When there is more than one antigen of interest, double or even triple labelling of tissue sections can be performed. The technique is the same as single labeling except that more than one antibody is used. The antibodies used must be developed in different species, and different chromogenic substrates or fluorescent dyes (fluorophores) must be used.

Once the tissue sections are stained, they must be dehydrated and cover slipped when chromogens are used. When fluorescent dyes are used, the dehydration procedure will cause loss of the fluorescence and so the sections are cover slipped without dehydration. Fluorescent dyes fade or bleach rapidly and therefore slides must be examined within a short period of time. Using special mounting media and storing the slides in the dark in a freezer can delay fading or bleaching. Xylene soluble mounting media is used in the case of chromogens and water soluble mounting media is used in the case of fluorophores.

For antibodies attached to a chromogen a conventional light microscope is used. For antibodies attached to a fluorescent dye (fluorophore), the reaction is visualized using a fluorescent microscope. In fluorescent microscopy, molecules that are excited via chemical or physical means emit light. Some atoms will absorb light at a particular wavelength and subsequently emit light of a particular longer wavelength. This is termed the fluorescence life time. A fluorescent microscope uses mirrors and filters that excite fluorophores within a sample of tissue. The resultant fluorescence is then transmitted to the eyepiece.

The tissues can be viewed using either a conventional fluorescent microscope or a confocal laser scanning microscope. In a conventional fluorescent microscope the section is bathed in light from a single light source, usually a xenon or mercury lamp. The resultant image is then viewed.

In confocal microscopy the section is scanned with one or more beams of light from a laser source. A photomultiplier tube detects the light generated and the image is then processed and generated by a computer. The advantages of confocal microscopy over conventional fluorescent microscopy is that depth of field can be controlled, background can be eliminated, serial optical sections can be collected from a section, and images with higher resolution can be obtained.

1.4.2 Western Blot

Western blot utilizes an antigen-antibody reaction to identify a particular protein within a mixture of proteins. The protein molecules are firstly separated using sodium dodecyl (lauryl) sulfate (SDS) polyacrylamide gel electrophoresis. Electrophoresis is the migration of particles within an electric field. The rate of movement of the particles is dependent on their size, their

shape, the strength of the electric field, and also on the ionic strength, viscosity and temperature of the medium in which the particles are submerged.

The sample tissue is macerated and filtered. The filtrate rich in the protein of interest is loaded onto a SDS polyacrylamide gel. When exposed to an electric current, proteins will migrate towards the cathode. The SDS denatures proteins and binds to the proteins resulting in the proteins having a negative charge since the SDS is anionic. By denaturing the proteins the proteins attain a linear configuration as the SDS disrupts the opposing electrical charges on the amino acid chains. Disruption of the protein tertiary structure is also attained via addition of 2-mercaptoethanol or dithiothreitol to the SDS. Therefore, all proteins will migrate linearly through the gel based on their weight and not on their tertiary structure or charge.

Following electrophoresis, the proteins are transferred to a nitrocellulose membrane. Electrophoretic transfer is most commonly used. The gel is placed in direct contact with a nitrocellulose membrane. A current is applied and the proteins migrate and bind to the nitrocellulose membrane. The membrane is then blocked using milk or serum, so that unreacted sites are blocked. The membrane is then incubated with an antibody specific for to the antigen of interest. Incubation times and antibody concentrations vary dependent on the antibody and the antigen. The membrane is then incubated in the secondary antibody that is attached to an enzyme.

The reaction is developed either by chemiluminescence or color development by addition of a substrate that reacts with the enzyme on the secondary antibody. Luminol is a commonly used luminescent agent. Oxidization of luminol occurs in the presence of horseradish peroxidase and hydrogen peroxide. Three-aminophthalate is produced which emits light. The membrane is then exposed to a radiographic film. An alternative to radiographic film is to use a CCD camera.

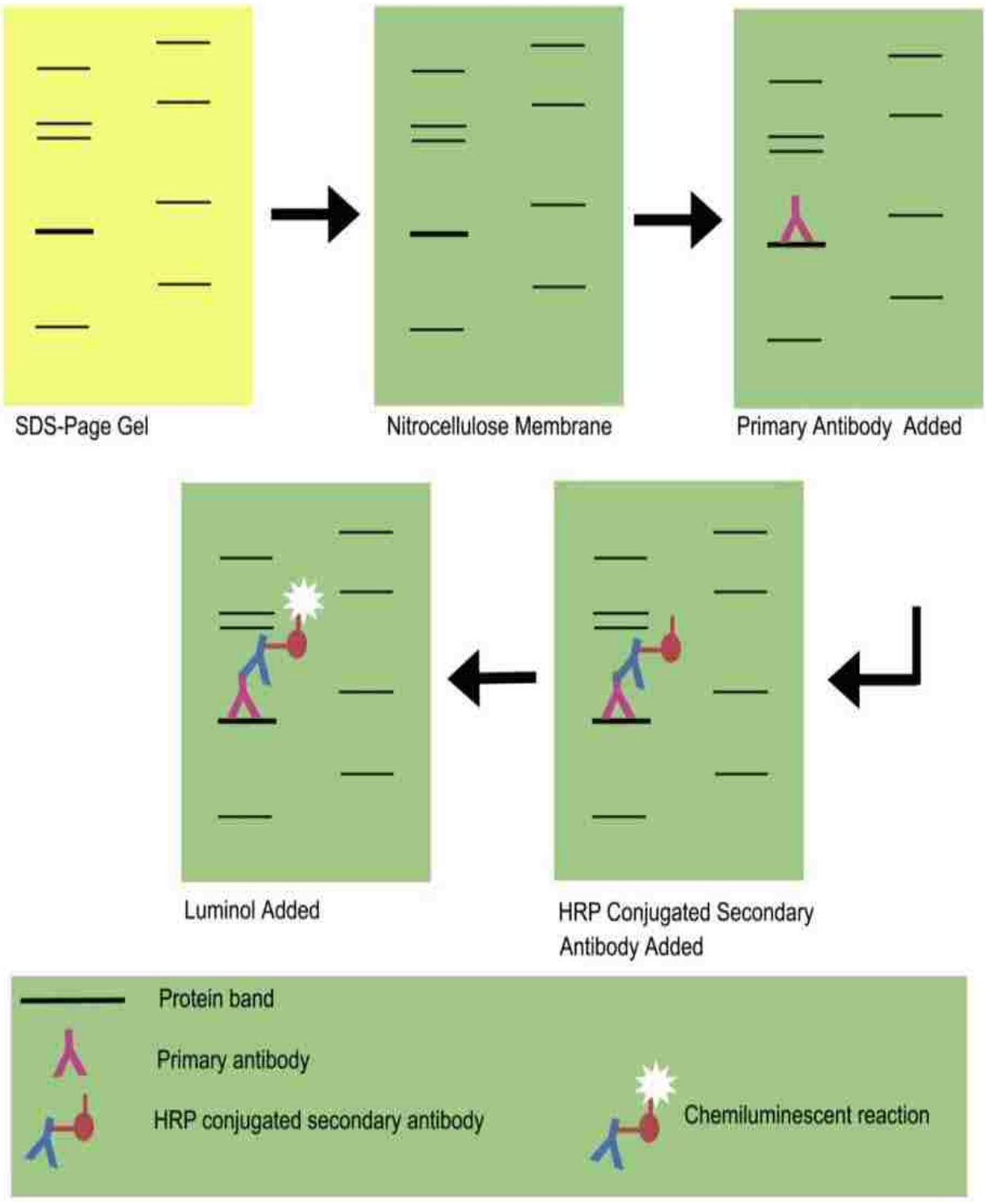

Figure 1.5 Schematic representation of the Western blot procedure

1.4.3 Reverse Transcriptase Polymerase Chain Reaction

Reverse transcriptase polymerase chain reaction (RT-PCR) is a highly sensitive method by which mRNA is detected and quantified (Singleton 2000). The first step is the production of a complementary strand of DNA (cDNA) on a RNA target (Singleton 2000). The cDNA is then used as a template for a PCR.

Firstly, RNA is isolated from the tissue of interest. The tissue is homogenized in a reagent containing phenol and guanidine thiocyanate which inhibits RNAse activity (Singleton 2000). The addition of bromochloropropane or chloroform causes separation of the homogenate into aqueous and organic phases (Singleton 2000). RNA partitions to the aqueous phase, DNA to the interphase, and proteins to the organic phase (Singleton 2000). Following the addition of isopropanol, RNA is precipitated from the aqueous phase (Singleton 2000).DNAse is added to destroy any DNA that may be present. RT-PCR is performed to obtain cDNA.

Primers are required for the PCR. A primer is a short strand of DNA or RNA needed for initiation of DNA synthesis using a DNA or RNA template (Singleton 2000). Primers are synthesized based on the known sequence of the gene of interest. The primers are usually 15-25 nucleotides in length (Singleton 2000). The primers must not include sequences that will allow primer to primer binding, or binding of one part of a primer to another part of the same primer (Singleton 2000).

It is important not to use primers with complementarity at the 3' of the primers as this will lead to primers acting as templates and the production of primer-dimers (Singleton 2000). In order for cDNA to be synthesized the primer binds to a specific site on the template thereby the primer determines which part of the template is to be copied. The primer is then extended by sequential addition of deoxyribonucleotides from its 3' end (Singleton 2000). The enzyme

responsible for this step is reverse transcriptase and the resultant product is a strand of cDNA (Singleton 2000). An RNAse destroys the RNA strand and a second strand of cDNA is produced (Singleton 2000). This double stranded cDNA then undergoes a PCR (Singleton 2000).

The PCR reaction mixture undergoes thermal cycling (Singleton 2000). Thermal cycling involves repeated exposure to a cycle of 3 levels of temperature: 1. Denaturation (separation of cDNA strands; 2. Annealing (binding of primers); 3. Extension (DNA synthesis by polymerase) (Singleton 2000). At the end of the reaction, the result is a PCR product. Confirmation and or quantification of the PCR product are then made.

The amplicon length is a specific length since the amplicon is delimited by a pair of primers (Singleton 2000). Therefore when run on an agarose gel, the amplicons from a specific PCR will localize at a specific location based on its weight (Singleton 2000). A standard or ladder is run at the same time.

The bands are detected by staining the gel with ethidium bromide. When the ethidium binds to DNA its fluorescence increases more than 20 times under ultraviolet light (Singleton 2000). SYBR® Green I fluoresces brightly at 530nm when it binds to double stranded DNA (Singleton 2000). It is added to the PCR mixture and as the amount of the product increases, so does the intensity of the fluorescence.

The fluorescence is monitored at the end of the extension stage. A curve is generated and a positive inflection indicates a positive PCR product (Singleton 2000). However, false positives can result if primer-dimers are present (Singleton 2000). Once confirmed, the PCR product is sequenced and the sequence is compared to known sequences on a database of sequences available on the NCBI website.

1.5 Antigens Used to Distinguish Between Synoviocyte Phenotypes

1.5.1 CD18

CD18 is a leukocyte integrin belonging to the leukocyte cell adhesion molecule that is only expressed on leukocytes (Danilenko et al. 1992). Integrins are a cell surface adhesive receptors involved in diverse cell functions which involve leukocyte adhesion and are therefore critical in the immune response (Danilenko et al. 1992). Cells positive for CD18 have been shown to be increased in joint capsular synovium from CrCL deficient stifles (Klocke et al. 2005). The number of CD18 cells correlated with the degree of arthritis (Klocke et al. 2005).

1.5.2 HSP25

Heat shock proteins (HSPs) are a family of proteins that play an important role in cellular defense and are up regulated in response to injury. Most HSPs are molecular chaperones that bind and stabilize proteins at intermediate stages of folding, assembly, translocation across membranes and degradation. Heat shock protein 25/27 is involved in regulation of actin assembly/disassembly. Up regulation of HSP25/27 has been shown to preserve neuronal function following nerve injury, and to protect the heart against ischemic-reperfusion injury in the mouse (Hollander et al. 2004, Sharp et al. 2006). Despite the normal protective role of HSPs, auto antibodies directed against them have been reported to play a role in immune mediated arthrides (Oda et al. 1994). Additionally HSP25/27 has been shown to be up regulated in canine mammary carcinomas and in human prostatic cancer (Horman et al. 1999). Heat shock protein 25/27 has also been shown to be up regulated in tissue development such as in adipogenesis, temperomandibular joint development, and in the development of skin (Ikeda et al. 2004, Duverger et al. 2005).

CHAPTER 2. CHARACTERIZATION OF NORMAL CANINE CRANIAL CRUCIATE LIGAMENT ASSOCIATED SYNOVIOCYTES*

2.1 Introduction

The Cranial cruciate ligament (CrCL) is highly conserved between species, and the canine stifle is an acceptable animal model for musculoskeletal investigations including but not limited to joint disease and CrCL healing and reconstruction (Chu et al. 2002, Lopez et al. 2003).

The structure, vasculature, composition, and function of the canine CrCL have been the focus of multiple investigations (Girgis et al. 1975, Arnoczky et al. 1977, Arnoczky 1983, Krauspe et al. 1992, Dragoo et al. 2003, Murray et al. 2004). Like the majority of mammalian CrCLs, The canine CrCL is intra-articular and extrasynovial since it is surrounded by a synovial membrane (Arnoczky et al. 1977, Arnoczky et al. 1979, Arnoczky 1983). While significant scientific focus has been dedicated to the canine CrCL, the synoviocytes surrounding it have received little attention.

Differentiation of synoviocyte phenotypes requires immunostaining or electron microscopy, and three synoviocyte phenotypes have been identified in the joint capsular synovium in several species (Barland et al. 1962, Barratt et al. 1977, Edwards et al. 1982, Stevens et al. 1990, Wilkinson et al. 1992, Kitamura et al. 1999, Ikeda et al. 2004, Klocke et al. 2005, Nagai et al. 2006).

The synoviocyte phenotypes identified include the type A (macrophage-like), type B (fibroblast-like), and an intermediate type (type C) (Barland et al. 1962, Barratt et al. 1977, Edwards et al. 1982, Stevens et al. 1990, Wilkinson et al. 1992, Kitamura et al. 1999, Ikeda et al. 2004, Klocke et al. 2005, Nagai et al. 2006).

*Reprinted by permission of the Journal of Orthopedic Research

To date, techniques used to characterize joint capsular synoviocytes have not been applied to CrCL associated synoviocytes. Expression of cathepsin K and tartrate resistant acid phosphatase (TRAP), both collagenolytic enzymes, are elevated in ruptured canine CrCLs and in joint capsular synovium from humans with rheumatoid arthritis (Hummel et al. 1998, Muir et al. 2002). It is not possible to distinguish between the synoviocyte phenotypes based on these enzymes since they are produced by both type A and type B synoviocytes (Drake et al. 1996, Hummel et al. 1998).

Synoviocytes normally maintain and protect the joint (Sledge 2001). Healthy CrCL hamstring grafts are surrounded by synovium indicating graft maturity and joint incorporation (Lopez et al. 2003). Though synoviocytes are normally supportive, they are also known to contribute to some disease processes (Zhu et al. 2006, Kontny et al. 2007). In rheumatoid arthritis, idiopathic arthritis, and CrCL rupture, type B synoviocytes express interleukins 6 and 8, prostaglandin E2, and nitrous oxide (Zhu et al. 2006, Kontny et al. 2007). While CrCL rupture in human is mostly due to trauma, many are spontaneous (Arendt et al. 1995).

Spontaneous CrCL rupture is the most common cause of CrCL damage in the canine (Vasseur et al. 1985, Hayashi et al. 2003). Characterization of canine CrCL synovicytes is important to understanding their potential contributions to CrCL health, disease, healing, and graft incorporation and maturation. CD18 is a highly conserved leukointegrin beta subunit that has been localized on canine synovial macrophages (Klocke et al. 2005). Rat temporomandibular joint type B synoviocytes express HSP25, a small heat shock protein (Ikeda et al. 2004). This study was designed to identify and quantify canine CrCL synoviocyte phenotypes based on immunohistochemical staining with CD18 and HSP25. We hypothesized that there are at least 2 synoviocyte phenotypes with distinct topographical distributions.

2.2 Materials and Methods

This study was performed in accordance with Institutional and National Institutes of Health regulations governing the treatment of vertebrate animals. Cranial cruciate ligaments were collected immediately post mortem from one randomly selected stifle of 4 intact female and 6 intact male dogs that were clinically healthy and that had no evidence of orthopedic disease. They were mixed breed young adults with a mean $\pm$ SD weight of 22.6 $\pm$ 0.45kg. Animals were euthanized for reasons unrelated to this study.

2.2.1 Immunohistochemistry

The CrCLs were aseptically harvested by transection at the origin and insertion. They were divided into two equal sagittal sections and fixed in 10% formalin. Three 7μm serial sections were cut from the axial and abaxial aspects of each sagittal section following paraffin embedding (Fig 2.1). Deparaffinized sections were immunostained for two different synoviocyte phenotypes using a murine monoclonal antibody against canine CD18 (PF Moore, Davis, CA) and a rabbit polyclonal antibody against murine heat shock protein 25 [HSP25 (Stressgen Bioreagents, Ann Arbor, MI)].

An auto-stainer (DAKO, Carpinteria, CA) was used for all double staining procedures. Following deparaffinization and rehydration, endogenous peroxidase was quenched with hydrogen peroxide. Antigen retrieval was carried out with heated citrate and proteinase K (Dako, Carpinteria, CA). Slides were blocked with normal horse serum (Vector Labs, Burlingame, CA) followed by incubation with anti-CD18 antibody (diluted 1:5). Following incubation with horse radish peroxidase (HRP) conjugated secondary antibody (DAKO EnVision, Dako, Carpinteria, CA), color was developed with a peroxidase substrate (DAB). Slides were next incubated with anti-HSP25 antibody (diluted 1:200) followed by incubation in a horseradish peroxidase

conjugated secondary antibody (DAKO EnVision, Dako, Carpinteria, CA).

The slides were incubated with a second peroxidase substrate (VIP, Vector Labs, Burlingame, CA). Positive controls for the CD18 and HSP25 were canine lymph node and murine urinary bladder, respectively. Negative controls were the canine CrCL with the primary antibody omitted. Slides were counterstained with methyl green (Vector Labs, Burlingame, CA).

2.2.2 Microscopy

For purposes of cell quantification, the Cranial and Caudal surfaces of each medial, central, and lateral sagittal section were evaluated in three equal transverse planes; proximal, middle, and distal for a total of 18 separate regions (Fig 2.1). Slides were evaluated at a magnification of 600x with light microscopy (Model DM5000, Leica Microsystems Inc., Bannockburn, IL). Digital photomicrographs of three representative fields were generated in each region and the digital images were exported as uncompressed tagged-image file format files (TIFF) at 400X400 dots per inch (dpi) and implemented in Adobe Photoshop v5.5 (Adobe Systems, Seattle, WA).

The software was used to quantify the number of pixels corresponding to each color of interest in the replicate images within each region. The software tolerance was adjusted to ensure that only intact cells with a clearly stained cytoplasm were counted. There were three colors of interest; brown, representing CD18 positive synoviocytes (CD18 +) within the cytoplasm; purple, representing synoviocytes that positively stained with the HSP25 antibody (HSP25+) within the cytoplasm and nucleus; and both purple and black, representing synoviocytes positively stained for both antibodies [double stained positive (DS+)] in which the nucleus was purple and the cytoplasm was black (combination of brown and purple). The mean proportional pixel count for each phenotype was the response variable used for statistical purposes.

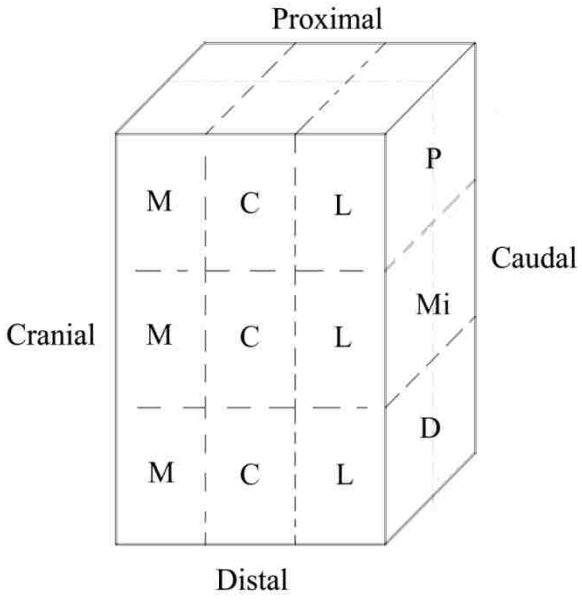

Figure 2.1 Schematic representation of regions evaluated within each CrCL. P = proximal, Mi = middle, D = distal, M = medial, C = central, and L = lateral.

2.2.3 Validation

The presence of HSP25 and CD18 in the canine CrCL was validated with western blot analysis, reverse transcriptase polymerase chain reaction (RT-PCR) and immunoelectron microscopy. Immunohistochemistry using light microscopy was performed on ten normal canine CrCLs. For western blot analysis, the CrCL was homogenized in phosphate buffered saline and heated to 95 ºC. The homogenate was centrifuged at room temperature and the supernatant was collected. For detection of HSP25, a reducing western blot method was used, however for CD18 a non reducing method was used.

Following resolution by electrophoresis, proteins were transferred to a nitrocellulose membrane (Biorad, Hercules, CA) and probed with either anti-HSP25 antibody or anti-CD18 antibody. Primary antibody was detected with an HRP conjugated goat anti rabbit antibody (1:1000) and an HRP conjugated horse anti murine antibody (1:2000) for HSP25 and CD18, respectively. Antibody complexes were imaged with a chemiluminescent analysis system (GE health care,

Buckinghampshire, UK) and the nitrocellulose membrane was exposed to a blue light sensitive film (Amersham, Piscataway, NJ). Canine lymph node (CD18) and murine urinary bladder (HSP25) were positive controls.

Total RNA was extracted from canine CrCL, murine heart and bladder, and canine lymph node tissue by homogenization in TRI reagent (Sigma, ST. Louis, MO), and cDNA was generated. (BD Biosciences, Palo Alto, CA). Primers were designed based on homologous regions between canine HSP27 (NCBI accession # UI9368.1) and murine HSP25 (NCBI accession # L11608), since anti murine HSP25 antibody cross reacts with the HSP27 protein according to the manufacturer. Primers for canine CD18 were designed using the available CD18 mRNA sequence (NCBI accession # AF181965). Primers were optimized and validated using real-time RT PCR SYBR Green™ (Clontech, Mountain View, CA) technology. Both amplicons were sequenced and compared to known sequences.

For detection of the CD18 epitope using immunoelectron microscopy, 10µm CrCL sections were immunostained with anti-CD18 antibody using the avidin-biotin technique as described previously.(Russinova et al. 2000). Following deparaffinization, antigen retrieval was carried out with heated citrate. Slides were blocked with goat serum followed by incubation with the anti-CD18 antibody (diluted 1:5). Following incubation with biotinylated goat anti murine secondary antibody (Electron Microscopy Sciences, Hatfield, PA), the sections were incubated in streptavidin colloidal gold with a 20nm particle size (EY Laboratories, San Mateo, CA). Slides were covered with epoxy resin and, following curing, the resin and attached tissue were removed from the slide. Thin 80µm sections were cut, placed on grids and stained with uranium acetate (Electron Microscopy Sciences, Hatfield, PA) and lead citrate (Electron Microscopy Sciences, Hatfield, PA). The positive control was canine lymph node and negative control was the CrCL with the primary antibody omitted.

For identification of the HSP25 antibody-epitope complex, a different technique was used. Following formaldehyde and glutaraldehyde fixation and embedding in LR white resin (Electron Microscopy Sciences, Hatfield, PA) 80μm sections of canine CrCL and murine urinary bladder were prepared. Proteinase K antigen retrieval was performed and sections were incubated with anti-HSP25 antibody (diluted 1:10) followed by incubation with a goat anti rabbit secondary antibody (diluted 1:50) conjugated to 10nm gold particles (Sigma-Aldrich, St. Louis, MO). Sections were stained with uranyl acetate and lead citrate and sections were imaged with a transmission electron microscope (Model JEM 1011, JEOL, Tokyo, Japan).

2.2.4 Statistical Analysis

The total pixel count for each phenotype was considered continuous and found to follow a normal distribution with failure to reject the null hypothesis of normality using the Shapiro-Wilk statistic at $p \leq 0.05$. The count and proportional count were summarized as mean +/- SD. The proportional pixel count was evaluated for a fixed effect of phenotype using a mixed linear model that included the random variance of canine distributed across all phenotypes. Where there was a significant effect of phenotype, ad hoc comparisons across phenotype were made using Scheffe's adjustment to maintain type I error at 0.05.

The proportional pixel count that stained for each phenotype within each of the regions was calculated and used for statistical analysis. The data did not follow a normal distribution. Transformation of the data failed. Dummy variables were created for each phenotype for a given region. A comparison among regions across phenotypes was made using the Kruskall-Wallis test with significance determined at $p<0.05$. Ad hoc comparisons were made using the Kruskall-Wallis procedure, maintaining type I error at 0.05. The median, quartiles and range of the regional pixel count and the regional pixel proportion is reported to summarize the data. PROCS

UNIVARIATE and PROC MIXED, PROC NPARIWAY were used for analysis (SAS v 9.1, SAS institute, Cary, NC).

2.3 Results

Three distinct synoviocyte populations were identified within the canine CrCL synovium with light microscopy: CD18 +, HSP25 +, and DS+ (Fig 2). The total pixel count for HSP25 + synoviocytes (57 ± 7.5 %) was significantly greater than the proportion of CD18 + synoviocytes (27 ± 8.2 %), which was significantly greater than the proportion of DS+ synoviocytes (16 ± 3.5%).

In a comparison of the mean (± SEM) pixel proportion within medial, central and lateral sections, HSP25+ synoviocytes were significantly greater than that DS+ synoviocytes in proximal, middle and distal regions and significantly greater than the CD18+ synoviocytes in middle and distal regions. (Table 2.1) CD18+ synoviocytes were significantly greater than DS+ synoviocytes in proximal and distal regions (Table 2.1).

In a comparison of the mean (± SEM) pixel proportion within cranial and caudal regions the HSP25+ synoviocytes were significantly greater than the DS+ synoviocytes in central and lateral regions. (Table 2.2) CD18+ synoviocytes were significantly greater than the DS+ synoviocytes in only the central region. (Table 2.2)

Western blotting with anti-CD18 yielded an immunoreactive band at approximately 160 kD. (Figure 2.3) The amplicon sequence was 98% homologous to that of canine CD18 (NCBI accession # AF181965). Western blotting with anti-HSP25 antibody yielded an immunoreactive band at approximately 27 kD in murine bladder and heart as well as canine CrCL extracts. (Figure 2.3B) The canine amplicon sequence was 85% homologous to that of murine HSP25

(NCBI accession # L11608). Immunoelectron microscopy revealed gold labeling of synoviocytes enveloping the CrCL with either anti-CD18 or anti-HSP25 antibodies. (Figure 2.4)

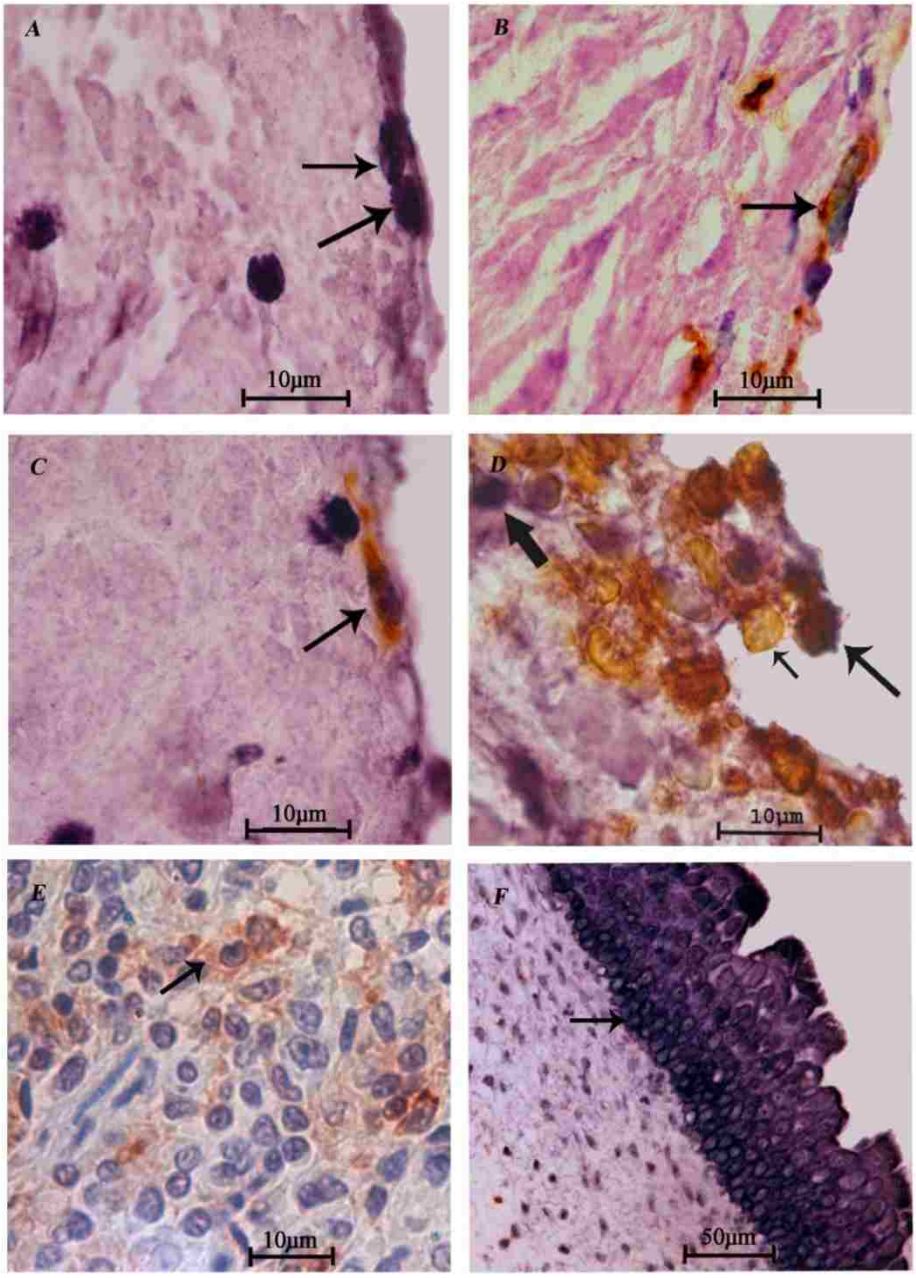

Figure 2.2 Photomicrographs of double immunostained CrCL sections. A: HSP25+ synoviocytes (arrows). B: CD18+ synoviocyte (arrow). C: DS+ synoviocyte (arrow). D: HSP25+ (thick arrow), CD18+ (short narrow arrow) and DS+ synoviocytes (narrow long arrow). E: CD18 positive control. F HSP25 positive control. (Magnification A-E: 600x, F: 200x, and counterstain A-F: methyl green)

Table 2.1 Mean (± SEM) pixel proportion for each phenotype within proximal, middle, and distal regions of medial, central, and lateral sections. Proportions with the same superscript are not significantly different.

	CD18	HSP25	DS
PROXIMAL	11 ± 1.8^{b}	16 ± 2.2^{ab}	0.09 ± 0.05^{c}
MIDDLE	9 ± 1.8^{bc}	25 ± 2.1^{a}	0.5 ± 0.3^{c}
DISTAL	12 ± 1^{b}	23 ± 2^{a}	1 ± 0.1^{c}

Table 2.2 Mean (± SEM) pixel proportion for each phenotype within medial, central, and lateral regions of cranial and caudal sections. Proportions with the same superscript are not significantly different.

	CD18	HSP25	DS
MEDIAL	6 ± 1.6^{b}	14 ± 2.8^{ab}	0.05 ± 0.03^{c}
CENTRAL	24 ± 10.7^{bc}	24 ± 1.4^{a}	0.7 ± 0.4^{c}
LATERAL	12 ± 2.2^{b}	27 ± 3.4^{a}	0.9 ± 0.4^{c}

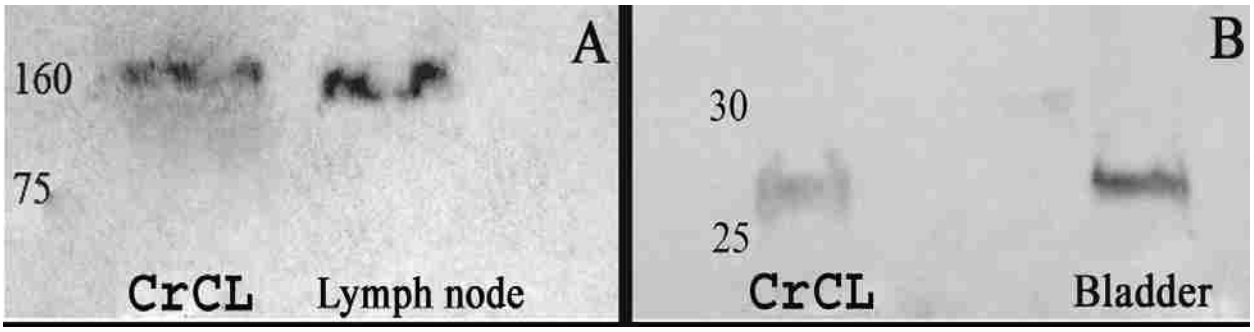

Figure 2.3 Western blot analyses of A: CD18 in control (canine lymph node) and canine CrCL tissues. CD18+ bands from both tissues are at approximately 160kD; and B: HSP25 in control (murine bladder) and canine CrCL tissues. Both bands are at approximately 27kD.

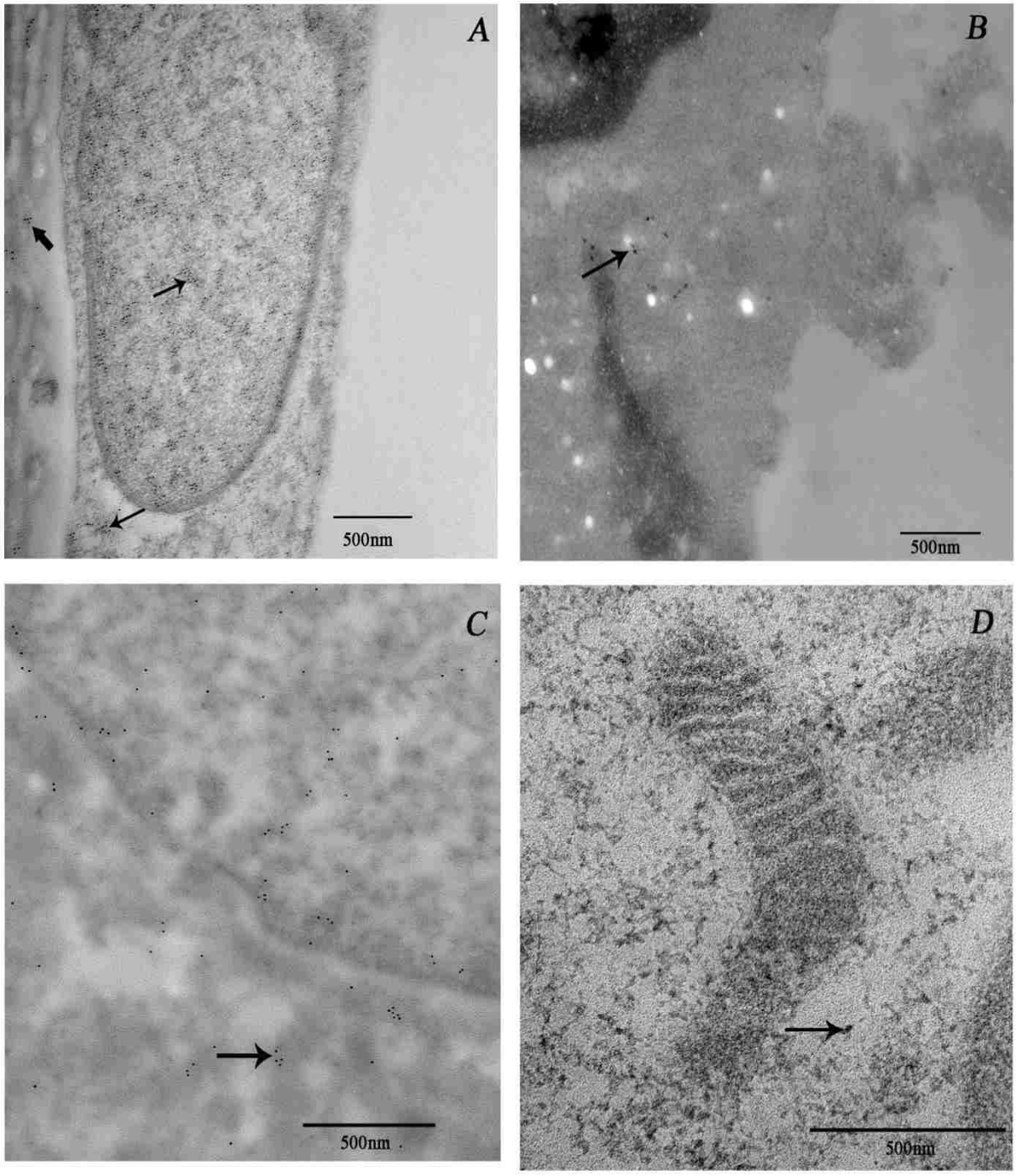

Figure 2.4 Transmission electron photomicrographs of immunogold labeling (arrows) of (A) canine CrCL synoviocytes with CD18 (30 000x); (B) canine CrCL synoviocytes with HSP25 (30 000x); (C) murine bladder with HSP25 (positive control, 40 000x); and (D) canine lymph node with CD18 (positive control, 60 000x). Gold labeling of the CD18 and HSP25 appear as black dots in the images.

2.4 Discussion

Three distinct synoviocyte phenotypes enveloping the normal canine CrCL were identified in this study with light microscopic immunostaining. The presence of CD18 and HSP25 epitopes in the canine CrCL was validated with western blot, RT-PCR, and TEM analysis. Based on quantification of regional immunostaining, distinct and consistent topographical distributions were identified for each synoviocyte phenotype. The two proteins selected for co-localization were based on current knowledge of synoviocyte phenotypes. There is evidence of at least two, and likely three joint capsular synoviocytes in a number of species; type A, type B and a transitional or stem cell like cell (type C) (Barland et al. 1962, Stevens et al. 1990, Wilkinson et al. 1992).

Small heat shock proteins play an important role in cellular defense and HSP25 is up regulated in response to injury (Hollander et al. 2004, Sharp et al. 2006). With light and TEM, HSP25 was localized to the cytoplasm and the nucleus consistent with previous study findings (Miron et al. 1991). Based on the fact that HSP25 is established as a type B joint capsular synoviocyte marker in the rat and human, it is likely that the labeled canine synovioycytes identified in this study are type B.

The CD18 antibody used in this study is specific for an epitope on common beta subunit of the leukocyte integrin family (Moore et al. 1992). The CD18 epitope is both cytoplasmic and membrane associated, and so, labeled cells are likely macrophage like (Pavalko et al. 1993). This is further supported by the knowledge that macrophage like synoviocytes make up 10-20% of the synovium of the human joint capsule which is similar to these study findings (Sledge 2001).

Synovioyctes that share characteristics of both type A and type B phenotypes have been previously identified (Barratt et al. 1977). The origin of canine synoviocytes has not been

established, however porcine synoviocyte have been shown to originate from the mononuclear phagocyte system and murine type A synoviocytes from bone marrow (Barratt et al. 1977, Edwards et al. 1982). It has been postulated that the type C macrophages are pluripotent and some consider that the type A, B, and C synoviocytes represent different functional states of the same cell (Fell et al. 1976, Barratt et al. 1977). The DS+ cells in our study may be analogous to the type C cells. Multipotent stem cells (MSC) have been identified within joint capsular synovium and the infrapatellar fat pad in the human stifle, and under cell culture conditions they have been shown to differentiate into chondrocyte, osteocyte, and adopocyte lineages (Bari et al. 1989, Wickham et al. 2003). Characterization and a means of identification of this cell type on the CrCL is important for future studies focused on the optimal conditions for desirable MSC differentiation.

HSP25 and CD18 antibodies have not been used extensively for routine canine CrCL immunostaining, so the presence of the proteins and mRNA expression was confirmed for both epitopes. Western blot analysis confirmed the presence of both proteins within the canine CrCL. HSP25 antibody cross-reacts with the HSP27 protein and, based on the western blot findings, the HSP27 epitope was isolated in this study (Engel et al. 1991). Further evidence for the presence of the proteins within the canine CrCL was obtained with RT PCR. Additional confirmation of localization of the epitopes was provided by the TEM. These validation steps substantiate the presence of CD18 and HSP25 epitopes on synoviocytes surrounding the CrCL.

The proportion of pixels stained for HSP25 + cells was significantly greater than for CD18 + synoviocytes or the double stained synoviocytes. Assuming that the HSP25 + synoviocytes have a fibroblastic function, a higher proportion of the phenotype would be expected for routine CrCL maintenance. Strain distribution along the length of the CrCL is not

uniform (Hirokawa et al. 2001). Additionally, the medial aspect of the CrCL is under greater stress than the lateral aspect with the most stress near the femoral insertion (Hirokawa et al. 2001). Therefore, variations in the proportions of each phenotype would be expected if stress or strain has an effect on the expression of particular phenotypes at specific regions. We did not observe any differences between the lateral and medial regions of the CrCL, however the proportion of pixels for HSP25+ synoviocytes was significantly greater than CD18+ or DS+ synoviocytes at the proximal region in all sections. Enumeration of synoviocyte phenotypes was necessary to obtain phenotypic proportions from normal CrCLs for purposes of potential comparison to damaged or diseased CrCLs in future studies.

Factors such as gender, anatomical, hormonal, and immune mediated processes have been implicated in the pathogenesis of spontaneous CrCL rupture though the precise pathogenesis is not known (Goldberg et al. 1982, Harner et al. 1994, Liu et al. 1997, Duval et al. 1999). Rupture of the CrCL is well described at the gross and histological level, and the synovium enveloping the CrCL has been described. However, a distinction between and the role of the synoviocytes within the synovium has received little attention (Arnoczky 1983, Hayashi et al. 2003, Hayashi et al. 2003). We have developed a novel mechanism to evaluate the CrCL that may facilitate understanding of the pathogenesis of CrCL rupture. Additionally, it may potentially be used to assess methods to augment CrCL graft reconstruction through acceleration of synovial encapsulation.

In conclusion, an immunohistochemical technique for the identification and quantification of three distinct synoviocyte phenotypes within the synovium enveloping the canine CrCL was developed and validated. Information may be useful for future studies surrounding CrCL disease, healing, and graft reconstruction. Additionally this information may

be useful for studies on synoviocyte phenotypes in canine models of CrCL disease. This novel approach to evaluation of the CrCL may significantly enhance future studies involving CrCL treatment and reconstruction.

CHAPTER 3. COMPARISON OF SYNOVIOCYTES ASSOCIATED WITH NORMAL, ARTIFICIALLY STRETCHED, AND NATURALLY DISRUPTED CANINE CRANIAL CRUCIATE LIGAMENTS

3.1 Introduction

The canine cranial cruciate ligament (CrCL) is composed of predominantly collagen and is surrounded by a 2-3 cell layer synovium (Arnoczky 1983). Synoviocytes normally maintain and protect the joint. Though synoviocytes are normally supportive, they are also known to contribute to some disease processes. In rheumatoid arthritis, idiopathic arthritis, and CrCL rupture, synoviocytes express interleukins 6 and 8, prostaglandin E2, and nitrous oxide (Zhu et al. 2006, Kontny et al. 2007). While significant scientific focus has been dedicated to the canine CrCL, the synoviocytes surrounding it have received little attention.

Microscopically, at least two synoviocyte phenotypes have been identified in the joint capsular synovium in several species. The synoviocyte phenotypes that have been identified include the type A (macrophage-like), type B (fibroblast-like), and an intermediate type (type C) (Stevens et al. 1990, Wilkinson et al. 1992, Kitamura et al. 1999, Ikeda et al. 2004, Lemburg 2004, Zhu et al. 2006). Similarly, in our lab we have identified and quantified three synoviocyte phenotypes within the synovium surrounding the CrCL in normal dogs (Vasanjee et al. 2008). Antibodies to CD18 and HSP25 epitopes were used to identify at least 3 synoviocyte phenotypes: CD18 positive (CD18+), HSP25 positive (HSP25+), and a population of cells in which co-localization of CD18 and HSP25 occurred (DS+) (Vasanjee et al. 2008). HSP25 synoviocytes are the predominant phenotype and DS synoviocytes are the least abundant in the synovium associated with the normal canine CrCL (Vasanjee et al. 2008).

The role that the synoviocytes play in health and disease of the CrCL is not known. Insight as to whether these synoviocytes play a role in CrCL disease may be obtained by

comparing the proportions of each of the phenotypes between diseased and normal CrCLs. The purpose of this study was therefore to identify and compare synoviocyte phenotypes proportions between normal, naturally partially disrupted, and artificially stretched canine CrCLs. We hypothesized that there would be three synoviocyte phenotypes in each group and that naturally disrupted and artificially stretched CrCLs would have a greater proportion of CD18 positive synoviocytes compared to normal CrCLs.

3.2 Materials and Methods

This study was performed in accordance with Institutional and National Institutes of Health regulations governing the treatment of vertebrate animals. Elongation of the CrCL was carried out in one randomly selected stifle from eight mature intact female mixed breed hounds with no clinical signs of orthopedic disease. The contra-lateral limb served as a non operated control. The CrCLs were elongated by approximately 25% using a specifically designed instrument using a standard open surgical approach (Lopez et al. 2006). Dogs were euthanized 12 weeks after surgery. Double fluorescent immunolabelling was carried out on each CrCL in order to determine the proportions of each synoviocyte phenotype.

3.2.1 Surgical CrCL Elongation

Following premedication with acepromazine (0.10 mg/kg, subcutaneously) and butorphanol (0.20 mg/kg, subcutaneously), the dogs were induced with thiopental (5%, intravenously [IV]) to effect. The dogs were then intubated and maintained on halothane in oxygen. Cefazolin (22mg/kg, IV) was administered at induction and repeated six hours later. The treated stifle was clipped and aseptically prepared for surgery. Following a medial arthrotomy, the patella was luxated laterally to allow examination of the CrCL and the joint. Single-interrupted sutures (2-0 Silk) were placed approximately 5mm apart in the CrCL mid-substance

with the distal most suture just proximal to the intermeniscal ligament. A bar type tension gauge (McMaster-Carr, Chicago, IL) was used to apply 2.5 N of tension to the distal aspect of the CrCL during measurements.

A specially designed device was used to stretch each CrCL midsubstance (Fig 3.1). The device had a hollow cylinder (7.5mm inner diameter; 10mm outer diameter) with a 2.5-mm-wide textured (80 grit) rim. Within the cylinder was a removable 10-gauge stainless-steel hook (5mm diameter, 2mm depth) attached to a retractable ratchet system that locked in place every 1.5mm. To effect tissue stretch, the hook was placed beneath each CrCL approximately equidistantly between sutures and retracted until it was entirely inside the cylinder. The textured surface of the cylinder was then engaged with the CrCL surface by pressing the device firmly against the CrCL.

Figure 3.1 Specifically designed device used to stretch the CrCL

With the stifle held in 135 degrees of flexion, the hook was retracted at a rate of 0.4–0.5mm/s to a displacement of approximately 3mm which was held for one minute then released. The joints were lavaged with 0.9% normal saline and sutured closed. Butorphanol tartrate

(0.2mg/kg IV) was administered once during anesthetic recovery and then intramuscularly every four hours for 24 hours as needed for analgesia. Etodolac (10mg/kg) was administered beginning 24 hours after surgery, and continued for seven days. Dogs were confined to 4 x 6 ft runs and taken for leash walks three times a day for the duration of the study.

Following euthanasia both the elongated and control CrCLs were aseptically harvested by transection at the origin and insertion, and fixed in 10% formalin. Gross evaluation of control CrCLs revealed four of the seven CrCL's to be partially disrupted. These CrCLs were classified as a naturally partially disrupted and included in the analyses.

3.2.2 Immunohistochemistry

Following embedding in paraffin, 7μm sagittal sections were cut from approximately the central aspect of each CrCL. The central aspect of the CrCL was chosen based on findings from a previous study that found no major differences between medial, central and lateral sections.(Vasanjee et al. 2008). Deparaffinized sections were immunostained for two different synoviocyte phenotypes using a murine monoclonal antibody against canine CD18 (PF Moore, Davis, CA) and a rabbit polyclonal antibody against murine heat shock protein 25 [HSP25 (Stressgen Bioreagents, Ann Arbor, MI)] that were validated in a previous study (Vasanjee et al. 2008).

Following deparaffinization and rehydration, endogenous peroxidase was quenched with hydrogen peroxide. Antigen retrieval was carried out with heated citrate and proteinase K (Dako, Carpinteria, CA) in order to expose CD18 and HSP25 antigens respectively. Slides were blocked with normal horse serum (Vector Labs, Burlingame, CA) followed by incubation with undiluted anti-CD18 antibody. All incubations were carried out in a humidified chamber to ensure sections would not dessicate.

Following incubation with biotinylated secondary antibody (DAKO EnVision, Dako, Carpinteria, CA), slides were incubated with Texas red conjugated streptavidin for 7 minutes. Slides were next blocked with normal goat serum, incubated with anti-HSP25 antibody (diluted 1:200) followed by incubation in a biotinylated secondary antibody (DAKO EnVision, Dako, Carpinteria, CA).

The slides were incubated with fluorescene conjugated streptavidin for 7 minutes. The slides were cover slipped and stored at -80º in the dark until microscopic analysis. All slides were evaluated by one of the investigators (SCV) who was aware of cruciate types. Positive controls for the CD18 and HSP25 were canine lymph node and murine urinary bladder, respectively. Negative controls were the canine CrCL with the primary antibody omitted.

3.2.3 Fluorescent Microscopy

For purposes of cell quantification, the medial and lateral aspects of the proximal, middle and distal regions were evaluated. Slides were evaluated at a magnification of 400x with a fluorescent microscope (Model DM5000, Leica Microsystems Inc., Bannockburn, IL). Digital photomicrographs were generated separately for each of the channels (Texas red and Fluoresceine). The digital images were exported as uncompressed tagged-image file format files (TIFF) at 400X400 dots per inch (dpi) and implemented in Adobe Photoshop CS (Adobe Systems, Seattle, WA). The separate images from each channel were merged, and the digital images were exported into Image-Pro Plus 5.0 (Media Cybernetics, Bethesda, MD).

The Adobe software was used to quantify the number of pixels corresponding to each color of interest within each region. There were three fluorescent colors of interest; red, representing synoviocytes that were CD18 +; green, representing synoviocytes that were HSP25+; and yellow, representing DS+ synoviocytes. The mean proportional pixel count

for each phenotype was the response variable used for statistical analysis.

3.2.4 Confocal Microscopy

Cellular localization and co-localization of CD18 and HSP25 was determined using confocal microscopy. Double immunofluorescent labeling as described above was carried out on a 10μm sections from an artificially stretched CrCL. Sections were examined with a TCS SP2 laser scanning microscope (Leica Microsystems, Exton, Pa.) fitted with a 63X Leica objective (1.4 numerical aperture; Planachromatic). Individual optical sections in the z axis, averaged three times, were collected in the different channels at 1024 by 1024 pixel resolution. Images analysis and co-localization fluorograms were generated and analyzed using the Leica confocal software.

3.2.5 Statistical Analysis

The proportion of all pixels that stained for each phenotype was calculated and used for statistical analysis. Log transformation normalized the data, verified by failure to reject the null hypothesis of normality at $p<0.05$ using the Shapiro-Wilk statistic. A comparison among regions and sections across phenotypes was made using a mixed linear model including the random variance of dog nested within groups. Significance was determined at $p<0.05$. Ad hoc comparisons were made using a Scheffe's adjustment, maintaining type I error at 0.05. The mean, standard deviation, median, quartiles and range of the pixel proportion is reported to summarize the data. PROCS UNIVARIATE and PROC MIXED, PROC NPARIWAY were used for analysis (SAS v 9.1, SAS Institute, Cary, NC).

3.3 Results

Three distinct synoviocyte populations were identified within the artificially stretched, naturally partially disrupted, and control canine CrCL synovium with fluorescent microscopy: CD18 +, HSP25 +, and DS+ (Fig 3.2).

The proportional pixel count for HSP25 + synoviocytes (57 ± 7.5 %) was significantly greater than the proportion of CD18 + synoviocytes (27 ± 8.2 %), which was significantly greater than the proportion of DS+ synoviocytes (16 ± 3.5%) in all groups. There was no significant difference in the proportions of each of the phenotypes between groups (tables 3.1, 3.2, and 3.3).

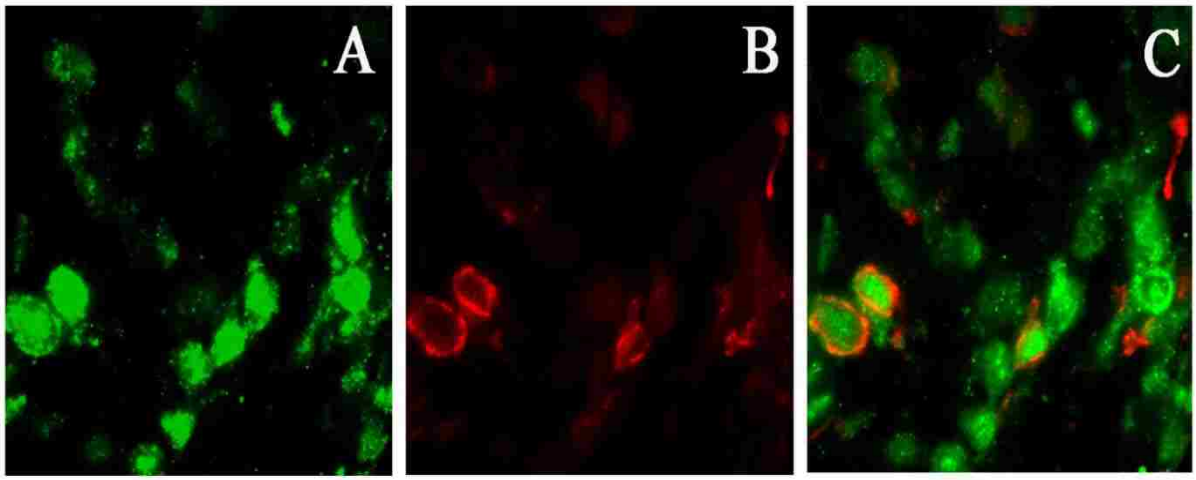

Figure 3.2 Photomicrographs of double immunostained CrCL sections A: HSP25+ synoviocytes. B: CD18+ synoviocytes. C: Merged image displaying co-localization of CD18 and HSP25 (DS+). (400X)

Table 3.1 Mean (± SEM) pixel proportion for each phenotype within proximal, middle, and distal central, and lateral regions for naturally partially disrupted CrCLs.

	CD18	**HSP25**	**DS**
PROXIMAL LATERAL	25 ± 19.7	73 ± 20.2	3 ± 0.6
PROXIMAL MEDIAL	29 ± 14.3	71 ± 14.7	1 ± 0.72
DISTAL LATERAL	16 ± 9.4	36 ± 20.6	19 ± 11.4
DISTAL MEDIAL	0.2 ± 0.4	3 ± 2	4 ± 1.8
MIDDLE	1 ± 0.7	89 ± 5.5	9 ± 5.3

Table 3.2 Mean (± SEM) pixel proportion for each phenotype within proximal, middle, and distal central, and lateral regions for normal CrCLs.

	CD18	HSP25	DS
PROXIMAL LATERAL	6 ± 4.2	74 ± 21.3	21 ± 17
PROXIMAL MEDIAL	28 ± 28.5	66 ± 26.6	5 ± 2.9
DISTAL LATERAL	4 ± 2.9	96 ± 3.2	0.3 ± 0.3
DISTAL MEDIAL	7 ± 6.9	76 ± 14.3	17 ± 14.1
MIDDLE	21 ± 12.4	76 ± 13.2	2.5 ± 1.6

Table 3.3 Mean (± SEM) pixel proportion for each phenotype within proximal, middle, and distal central, and lateral regions for artificially stretched CrCLs.

	CD18	HSP25	DS
PROXIMAL LATERAL	16 ± 13.8	75 ± 12.8	8.5 ± 2.9
PROXIMAL MEDIAL	12 ± 8.1	76 ± 8.8	11 ± 4.9
DISTAL LATERAL	2 ± 1.1	91 ± 4.8	7.1 ± 4.8
DISTAL MEDIAL	13 ± 9.5	81 ± 11.4	5.6 ± 4.1
MIDDLE	3.3 ± 2.9	93 ± 3.9	4 ± 2.9

Confocal laser microscopy confirmed the presence 3 synoviocyte phenotypes and generation of a fluorogram revealed co-localization of CD18 and HSP25 epitopes to the same cell (DS+ synoviocytes). The CD18+ staining was represented by the red staining and the HSP25 staining was represented by the green staining (Fig 3.3). Distinct red and green regions were evident within the fluorogram. The red region represented CD18+ staining and the green region represented HSP25+ staining indicating localization of CD18 and HSP25 epitopes to different regions within the same cell.

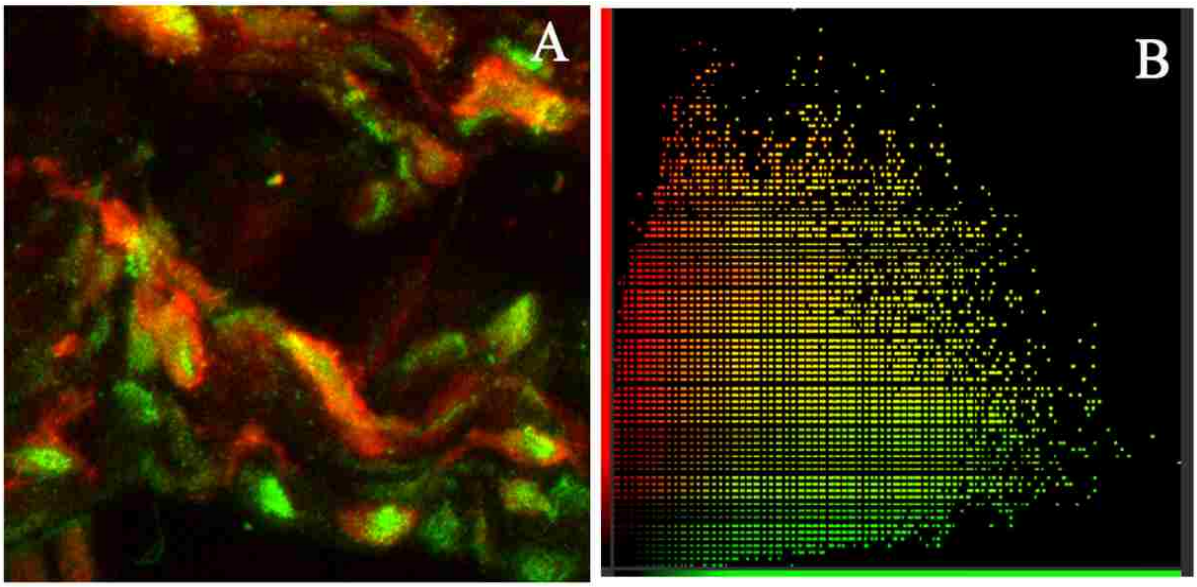

Figure 3.3 A. Confocal photomicrograph of double immunostained CrCL section (400X). B. Fluorogram depicting co-localization (B).

3.4 Discussion

We have used immunohistochemistry to identify and characterize three distinct synoviocyte phenotypes (CD18+, HSP25+, and DS+) enveloping the normal and abnormal canine CrCL. Co-localization of CD18 and HSP25 (DS+) to the same cell rather than to the same epitope was confirmed with confocal laser microscopy. We previously identified and validated the three synoviocyte phenotypes identified in the current study. However, fluorescent microscopy provided additional information with regards to characterization of co-localization.

The pathogenesis of CrCL rupture in dogs is not known. In order to gain insight into CrCL rupture, the CrCL has been evaluated extensively at the molecular and cellular levels. For instance, fibroblast shape and numbers within the core of the CrCL and concentrations of enzymes such as cathepsin K, have been shown to differ between normal and ruptured canine CrCLs (Murray 2000, Muir et al. 2002, Hayashi et al. 2003). The core of the CrCL does not come into contact with the synovial fluid since the CrCL is enveloped by a synovial membrane.

Antibodies to collagen types that make up the core of the CrCL have been detected in the synovial fluid from canine stifles with CrCL ruptures.(de Rooster et al. 2000). It is therefore possible that disruption of the CrCL associated synovial membrane may lead to immune complex formation between the CrCL collagen and the collagen antibodies from the synovium leading to degeneration and subsequent rupture of the CrCL. Thus by studying the CrCL associated synovium in normal and diseased CrCLs may provide information into the pathogenesis of CrCL rupture.

As previously reported, the proportion of pixels stained for HSP25 + cells was significantly greater than that for CD18 + synoviocytes or the DS+ synoviocytes in normal CrCLs. Assuming that the HSP25 + synoviocytes have a fibroblastic function, a higher proportion would be expected for routine CrCL maintenance. Conversely, given the likely phagocytic function of the C18+ synoviocytes, the proportion of pixels stained for CD18+ synoviocytes would be expected to be greater in diseased compared to normal CrCLs. We did not detect any differences between normal and diseased CrCLs for the proportion of CD18+, or for the other two synoviocyte phenotypes. The proportion of HSP25+ synoviocytes was the greatest in all CrCLs with the DS+ synoviocytes the least.

There are several possibilities as to why we did not detect differences in the proportion for each synoviocyte phenotype between diseased and normal CrCLs. Changes in the synoviocyte proportions may occur over time and therefore evaluation of multiple time points may be necessary to detect any differences. Secondly, our sample sizes for each CrCL type were small. An increased sample size may be necessary to detect differences. Thirdly, there may not be differences between diseased and normal CrCLs. While our model of CrCL disease does not represent natural disease, the partially disrupted CrCLs were as a result of natural disease.

The current study utilized fluorescent microscopy to detect the synoviocytes. However, a previous study utilized light microscopy. Identification of DS+ synoviocytes was easier when fluorescence was used. Confocal laser microscopy was used to characterize the co-localization in DS+ synoviocytes. Based on the fluorogram generated, CD18 and HSP25 antibodies in DS+ synoviocytes co-localized to different epitopes in the same cell. This finding suggests that the DS+ synoviocyte may in fact be a stem cell that shares characteristics of both CD18+ and HSP25+ synoviocytes.

We developed and validated a fluorescent immunohistochemical technique for the identification and quantification of three distinct synoviocyte phenotypes within the synovium enveloping the normal and diseased canine CrCL. All three synoviocyte phenotypes are present in both diseased and normal CrCLs and are present in similar proportions across normal and diseased CrCLs.

CHAPTER 4. CONCLUSION

Immunohistochemistry was used to identify and characterize three distinct synoviocyte phenotypes (CD18+, HSP25+, and DS+) enveloping the normal and abnormal canine CrCL in this study. We have validated these techniques using western blot, immunoelectron microscopy, confocal microscopy and RT-PCR.

Identification of synoviocyte phenotypes enveloping the CrCL in any species has not been previously reported in the literature. However, synoviocytes within the joint capsular synovium have been identified in multiple species (Barland 1962, Barland et al. 1962, Barratt et al. 1977, Burmester et al. 1983, Stevens et al. 1990, Kitamura et al. 1999, Ikeda et al. 2004, Klocke et al. 2005). It is not known whether synoviocytes within the joint capsule are identical to those enveloping the CrCL. Studies comparing these synoviocytes in different regions of the stifle are warranted.

The synovium has an important role in maintaining joint health. It is responsible for nourishing the joint (Walsh 1997, Sledge 2001). The importance of the synovium is highlighted in arthropathies such as rheumatoid arthritis and osteoarthritis in which the amount of hyaluronic acid is decreased in the synovial fluid (Yoshida et al. 2004). Hyaluronic acid is produced by fibroblast-like synovioctes and is responsible for joint lubrication and homeostasis (Yoshida et al. 2004). Hyaluronic acid inhibits prostaglandin synthesis, free radical damage, and enzyme degradation (Yoshida et al. 2004). This vital role may be one reason why the HSP25 synoviocyte phenotype was the predominant phenotype within the synovium enveloping the CrCL in our studies. Damage to this synovium via trauma, an immune mediated process, or secondary to stifle instability will reduce the amount of hyaluronic acid within the joint predisposing it to pathologic processes.

In our studies, the HSP25+ synoviocyte was the predominant phenotype surrounding both normal and diseased CrCLs. Based on the literature, and also based on the fact they were the predominant phenotype, the HSP25+ synoviocytes most likely represent the fibroblast-like synoviocytes. If damage to a CrCL results in reduction of the number of fibroblast-like synoviocytes, then we should have seen a lower proportion of HSP25+ synoviocytes from abnormal CrCLs. However, no significant differences were present. The synoviocyte proportions may be dynamic and difference may only be detected with evaluation at multiple time points. Although heat shock proteins have roles in both health and disease, a link between CrCL rupture and HSP25 is yet to be identified.

Since the CD18 antigen is present on leukocytes such as macrophages, the most likely synoviocyte phenotype labeled with the anti CD18 antibody is the macrophage-like synoviocyte. Macrophage-like synoviocytes, similar to other types of macrophages are phagocytic in nature. They contain degradative enzymes such as nonspecific esterase, acid phosphatase, and cathepsins B, D, and L (Yoshida et al. 2004). Macrophage-like synoviocytes degrade hyaluronic acid (Yoshida et al. 2004). For these reasons, the proportion of macrophage-like synoviocytes within the synovium are expected to be low in the normal CrCL. In the synovium encompassing normal CrCLs, the proportion of synoviocytes staining CD18+ were significantly lower than for HSP25+. Increased CD18+ staining would be expected to be increased at high stress areas such as sites of attachment or insertion of the CrCL. Increased staining was not seen in these regions.

As expected, the numbers of CD18+ synoviocytes within joint capsular synovium from dogs with CrCL rupture are increased when compared to normal joint capsular synovium (Klocke et al. 2005). The CD18+ synoviocytes numbers are higher the greater degree of

osteoarthritis (Klocke et al. 2005). This suggests that the CD18+ synovioctes may be responsible for modulating the progression of osteoarthritis via degradative enzymes and inflammatory mediators (Yoshida et al. 2004). Given their phagocytic nature, the numbers of CD18+ synoviocytes would be expected to be higher in abnormal CrCLs as retraction and resorption of the CrCL occurs following injury.(Murray 2000, Hayashi et al. 2003). However, no significant differences between normal and abnormal CrCLs were seen in our study.

Further studies are needed to determine if differences are noted when sampling at different time points. We evaluated the abnormal CrCLs 12 weeks after injury. A previous study revealed partial loss of the CrCL fiber matrix by 12 week after injury (Hayashi et al. 2003). It is not known whether the macrophage-like synoviocytes were responsible for this, but it does support the need to evaluate the CrCLs prior to 12 weeks when active damage to the CrCL is most likely occurring.

We have shown that a third phenotype, the DS+ synoviocyte has both CD18 and HSP25 antigens. This synoviocyte may represent the type C synoviocyte. Using confocal microscopy, we have shown that the antigens are present on different parts of the cell. The CD18 antigen is present on the cell membrane and the HSP25 antigen is present in both the cytoplasm and the nucleus. Given that the DS+ synoviocytes share characteristics of the CD18 and the HSP25 synoviocytes, the DS+ synoviocytes may represent a transitional phenotype that is a pluripotent stem cell with phenotypic plasticity. It has been postulated that type C synoviocytes are pluripotent, and some consider that the type A, B, and C synoviocytes represent different functional states of the same cell.(De Bari et al. 2001).

Mesenchymal stem cells have been identified in the human join capsular synovium (De Bari et al. 2001, Shirasawa et al. 2006). These stem cells are comparable to bone marrow derived

stem cells with respect to expansion ability (Sakaguchi et al. 2005). Synovium mesenchymal stem cells isolated from the synovium have excellent potential for differentiation into fat, cartilage and bone (Sakaguchi et al. 2005, Shirasawa et al. 2006). The DS+ synoviocytes in our study may represent a stem cell. Isolation and expansion of the DS+ synoviocyte phenotype in culture is warranted to determine if it is a stem cell.

Intra-articular infusion of bone marrow derived MSCs into rat joints with artificially created partial CrCL tears results in healing of the CrCL (Kanaya et al. 2007). Similar healing does not occur in control joints (Kanaya et al. 2007). A similar study is warranted in canine joints but with both artificially created and naturally partially ruptured CrCLs. A mechanism would need to be developed to ensure that the infused MSCs remain in the joint and close to the damaged portion of the CrCL for an extended period of time.

Light and fluorescent microscopy was used to identify the synoviocyte phenotypes. In the first study, light microscopy and chromogens were used. The number of different colored chromogens available is limited. Also, not all chromogens are compatible with each other, thus further limiting the number of chromogens that can be used concurrently. When double immunolabelling is carried out using chromogens, the chromogens must be easily distinguishable from each other. We used a purple and a brown chromogen. Though we were easily able to distinguish synoviocytes that solely stained CD18+ from those that solely stained HSP25+, it was difficult at times, to distinguish between the DS+ and the HSP25+. Adobe Photoshop software was therefore employed. Color subtraction was used to count the number of pixels corresponding to each color of interest. Once individual synoviocytes were identified, the Adobe Photoshop software's tolerance was adjusted and the wand tool was used to identify each color of interest. The result was a pixel count for each color of interest.

In the subsequent study, in order to clearly distinguish each phenotype, fluorescent immunolabelling was employed. The fluorescent dyes attached to each of the antibodies were of a different wavelength and therefore by using different filters, each phenotype was clearly identified. This appeared to be a more accurate assessment of staining for each phenotype proportion. It was difficult to identify individual synoviocytes, and hence the actual numbers of cells were not counted, but instead the pixels corresponding to each color of interest were determined using Image Pro software. Therefore our technique actually quantified and compared the proportions of CD18 and HSP25 localization or co-localization and not the actual numbers of individual synoviocytes. Given that the CD18 only stained the membrane and cytoplasm, and the HSP25 both the nucleus and cytoplasm, the pixel value may not be a reflection of the number of synoviocytes. For example, if the total pixel value for 3 CD18+ synoviocytes is 25, a single HSP25+ synoviocyte pixel value could be greater than 75.

The stifle joint capsular synovium in human cases of rheumatoid arthritis (RA) has been extensively studied. In RA, the synovium is characterized by extensive proliferation of fibroblast–like cells. These fibroblast-like cells produce interleukins and therefore are thought to be involved in the inflammatory process in RA (Harada et al. 1999). Macrophages present within the synovium also produce inflammatory mediators (Harada et al. 1999). It is not clear from these previous studies whether the macrophages originate from the synovium or if they originate from the vascular system. Whether this is similar to other forms of arthritis is not known, but does indicate that the synoviocytes are relatively quiescent under normal conditions but highly active during disease. Synthesis of interleukins and other inflammatory mediators from the synoviocytes surrounding the CrCL needs to be investigated. Determination of protein levels and mRNA levels of each of the interleukins warrants investigation to determine if in fact the

inflammatory mediators are produced from CrCL associated synoviocytes in CrCL rupture. This can be accomplished by performing RT-PCR and protein analysis on CrCL associated synovium as well on cultured synoviocytes.

Immunohistochemistry has been used to evaluate the efficacy of various treatments in human patients with RA. A marker of human macrophage-like synoviocytes, CD68 has been used to determine the effects of steroids, gold compounds, leflunomide, and methotrexate on these cells (Yanni et al. 1994, Gerlag et al. 2004, Haringman et al. 2005, Bresnihan et al. 2007, Gerlag et al. 2007). The number of macrophage-like synoviocytes decreased with each of these treatments, and there was a positive correlation with clinical symptoms. These studies indicate that the macrophage-like synoviocytes play a role in the synovitis and that by modulating their numbers, clinical improvement is seen. To determine if the same holds true for dogs with CrCL rupture, studies need to be carried out in which dogs with partial cranial cruciate ligament rupture are treated with various drugs that will modulate the synoviocyte phenotypes to determine if healing of the CrCL occurs. Similar results would be expected if CrCL rupture is truly an immune mediated process as is RA.

Before clinical studies are carried out canine synoviocyte cell lines of each phenotype that are stable and with an appropriate life span need to be established. The CrCL associated synoviocytes must be harvested such that contamination of other cells from the rest of the CrCL will not occur. Optimal conditions will need to be established to ensure propagation of each synoviocyte phenotype. The immunohistochemical techniques that we have developed will need to be employed to identify and monitor each synoviocyte phenotype. Growth of the various synoviocyte phenotypes within the same culture will be ideal so that characteristics of each phenotype under various conditions can be studied. Synthesis and expression of interleukins,

matrix metalloproteinases, and acute phase proteins have been evaluated using RA synoviocyte cell lines (Han et al. 2006, Mullan et al. 2006). Response to treatment with various drugs has also been evaluated (Haupt et al. 2005, Han et al. 2006). These studies with RA synoviocyte cell lines indicate that similar studies using CrCL rupture cell lines is plausible.

Synovial fluid from dogs with CrCL rupture contains antibodies to collagen (Bari et al. 1989, de Rooster et al. 2000). Since the CrCL is predominantly composed of collagen, this may suggest an auto-immune response targeting the CrCL. It is not known whether these antibodies are secondary to CrCL rupture or if CrCL rupture is secondary to development of these antibodies. Since the CrCL is surrounded by the synovium, it would not be possible for antibodies present in the synovial fluid to come into contact with the collagen unless damage was to occur to the synovium. Damage to the synovium will expose the CrCL to the joint fluid environment. The body may now see the previously unexposed CrCL proteins as foreign antigens. Antibodies would then be generated. Immune complexes may then deposit on the CrCL resulting in weakening and destruction of the CrCL. Alternatively, antibodies generated elsewhere in the body may gain access to the joint fluid or even the blood stream. These antibodies may then disrupt the synovium.

The presence of antibodies targeting the synoviocytes needs to be investigated to determine if an immune response that causes damage to the synovium surrounding the CrCL is in fact present and the origin of these antibodies needs to be determined. Western blot or an enzyme linked immunosorbant assay (ELISA) would be used to detect any antibodies. Since we know that the CrCL associated synoviocytes have CD18 or HSP25 antigens, the presence antibodies to these antigens in synovial fluid and serum needs to be evaluated. In conclusion, we have developed and validated a novel mechanism to evaluate the canine CrCL synoviocytes

that may facilitate understanding of the pathogenesis of CrCL rupture in future studies. The synoviocytes associated with the joint capsule have been identified previously in several species, however, as far as we know, this is the first time that synoviocytes associated the CrCL have been identified. This information will provide an alternate approach to understanding the pathogenesis of CrCL rupture. The ultimate goal is to prevent CrCL rupture, thereby mitigating animal and human morbidity as well as eliminating the financial burden.

BIBLIOGRAPHY

Aiken S, Kass, P., Toombs, J. Intercondylar notch width in dogs with and without cranial cruciate ligament injuries. VCOT 1995;8:128-132.

Anderson AF, Lipscomb AB, Liudahl KJ, et al. Analysis of the intercondylar notch by computed tomography. Am J Sports Med 1987;15:547-552.

Arendt E, Dick R. Stifle injury patterns among men and women in collegiate basketball and soccer. NCAA data and review of literature. Am J Sports Med 1995;23:694-701.

Arnoczky SP. Anatomy of the anterior cruciate ligament. Clin Orthop Relat Res 1983:19-25.

Arnoczky SP, Marshall JL. The cruciate ligaments of the canine stifle: an anatomical and functional analysis. Am J Vet Res, 1977;1807-1814.

Arnoczky SP, Rubin RM, Marshall JL. Microvasculature of the cruciate ligaments and its response to injury. An experimental study in dogs. J Bone Joint Surg Am 1979;61:1221-1229.

Arnoczky SP, Rubin, R.M., and Marshall, J. L. Microvasculature of the cruciate ligaments and its response to injury. An experimental study in dogs. J Bone Joint Surg Am 1979;61:1221-1229.

Arnoczky SP, Torzilli P., and Marshall, J.L. Biomechanical evaluation of anterior cruciate ligament repair in the dog. Am J Vet Res 1977;38:1807-1814.

Bari AS, Carter SD, Bell SC, et al. Anti-type II collagen antibody in naturally occurring canine joint diseases. Br J Rheumatol 1989;28:480-486.

Barland P, Novikoff AB, Hamerman D. Electron microscopy of the human synovial membrane. J Cell Biol 1962;14:207-220.

Barland P, Novikoff, A.B., and Hamerman, D. Electron microscopy of the human synovial membrane. J Cell Biol 1962;14:207-220.

Barratt ME, Fell HB, Coombs RR, et al. The pig synovium, II. Some properties of isolated intimal cells. J Anat 1977;123:47-66.

Blankevoort L, Huiskes R. Validation of a three-dimensional model of the stifle. J Biomech 1996;29:955-961.

Bresnihan B, Gerlag DM, Rooney T, et al. Synovial macrophages as a biomarker of response to therapeutic intervention in rheumatoid arthritis: standardization and consistency across centers. J Rheumatol 2007;34:620-622.

Bryant-Greenwood GD, Yamamoto SY. Control of peripartal collagenolysis in the human chorion-decidua. Am J Obstet Gynecol 1995;172:63-70.

Burmester GR, Dimitriu-Bona A, Waters SJ, et al. Identification of three major synovial lining cell populations by monoclonal antibodies directed to Ia antigens and antigens associated with monocytes/macrophages and fibroblasts. Scand J Immunol 1983;17:69-82.

Chu Q, Lopez MJ, Hayashi K, et al. Elevation of a collagenase generated type II collagen neoepitope and proteoglycan epitopes in synovial fluid following induction of joint instability in the dog. Osteoarthritis Cartilage 2002;10:662-669.

Cumps ED, Verhagen E, Annemans L, et al. Injury risk and socio-economic costs resulting from sports injuries in Flanders. Data derived from Sports Insurance Statistics 2003. Br J Sports Med 2007.

Danilenko DM, Moore PF, Rossitto PV. Canine leukocyte cell adhesion molecules (LeuCAMs): characterization of the CD11/CD18 family. Tissue Antigens 1992;40:13-21.

De Bari C, Dell'Accio F, Tylzanowski P, et al. Multipotent mesenchymal stem cells from adult human synovial membrane. Arthritis Rheum 2001;44:1928-1942.

de Rooster H, Cox E, van Bree H. Prevalence and relevance of antibodies to type-I and -II collagen in synovial fluid of dogs with cranial cruciate ligament damage. Am J Vet Res 2000;61:1456-1461.

Demirag B, Sarisozen B, Durak K, et al. The effect of alpha-2 macroglobulin on the healing of ruptured anterior cruciate ligament in rabbits. Connect Tissue Res 2004;45:23-27.

Doverspike M, Vasseur PB, Harb MF, et al. Contralateral cranial cruciate ligament rupture: incidence in 114 dogs. J Am Anim Hosp Assoc 1993;29:167-170.

Dragoo JL, Lee RS, Benhaim P, et al. Relaxin receptors in the human female anterior cruciate ligament. Am J Sports Med 2003;31:577-584.

Drake FH, Dodds RA, James IE, et al. Cathepsin K, but not cathepsins B, L, or S, is abundantly expressed in human osteoclasts. J Biol Chem 1996;271:12511-12516.

Duval JM, Budsberg SC, Flo GL, et al. Breed, sex, and body weight as risk factors for rupture of the cranial cruciate ligament in young dogs. J Am Vet Med Assoc 1999;215:811-814.

Duverger O, Morange M. Heat shock protein 25 plays multiple roles during mouse skin development. Cell Stress Chaperones 2005;10:268-277.

Edwards JC, Willoughby DA. Demonstration of bone marrow derived cells in synovial lining by means of giant intracellular granules as genetic markers. Ann Rheum Dis 1982;41:177-182.

Engel K, Knauf U, Gaestel M. Generation of antibodies against human hsp27 and murine hsp25 by immunization with a chimeric small heat shock protein. Biomed Biochim Acta 1991;50:1065-1071.

Fell HB, Glauert AM, Barratt ME, et al. The pig synovium. I. The intact synovium in vivo and in organ culture. J Anat 1976;122:663-680.

Gerber C, Matter, P. Biomechanical analysis of the stifle after rupture of the anterior cruciate ligament and its primary repair. An instant-centre analysis of function. J Bone Joint surg Br 1983;65-B:391-399.

Gerlag DM, Boyle DL, Rosengren S, et al. Real-time quantitative PCR to detect changes in synovial gene expression in rheumatoid arthritis after corticosteroid treatment. Ann Rheum Dis 2007;66:545-547.

Gerlag DM, Haringman JJ, Smeets TJ, et al. Effects of oral prednisolone on biomarkers in synovial tissue and clinical improvement in rheumatoid arthritis. Arthritis Rheum 2004;50:3783-3791.

Girgis FG, Marshall JL, Monajem A. The cruciate ligaments of the stifle joint. Anatomical, functional and experimental analysis. Clin Orthop Relat Res 1975:216-231.

Goldberg VM, Burstein A, Dawson M. The influence of an experimental immune synovitis on the failure mode and strength of the rabbit anterior cruciate ligament. J Bone Joint Surg Am 1982;64:900-906.

Goodfellow J, O'Connor J. The mechanics of the stifle and prosthesis design. J Bone Joint Surg Br 1978;60-B:358-369.

Greenhalgh DG, Sprugel KH, Murray MJ, et al. PDGF and FGF stimulate wound healing in the genetically diabetic mouse. Am J Pathol 1990;136:1235-1246.

Halata Z, Rettig T, Schulze W. The ultrastructure of sensory nerve endings in the human stifle joint capsule. Anat Embryol (Berl) 1985;172:265-275.

Han SK, Jeon SJ, Miyazawa K, et al. Enhancement of anti-inflammatory tendency by SB203580, p38alpha specific inhibitor, in human fibroblast-like synoviocyte cell line, MH7A. Rheumatol Int 2006;26:972-978.

Harada S, Yamamura M, Okamoto H, et al. Production of interleukin-7 and interleukin-15 by fibroblast-like synoviocytes from patients with rheumatoid arthritis. Arthritis Rheum 1999;42:1508-1516.

Haringman JJ, Gerlag DM, Zwinderman AH, et al. Synovial tissue macrophages: a sensitive biomarker for response to treatment in patients with rheumatoid arthritis. Ann Rheum Dis 2005;64:834-838.

Harner CD, Paulos LE, Greenwald AE, et al. Detailed analysis of patients with bilateral anterior cruciate ligament injuries. Am J Sports Med 1994;22:37-43.

Haupt JL, Frisbie DD, McIlwraith CW, et al. Dual transduction of insulin-like growth factor-I and interleukin-1 receptor antagonist protein controls cartilage degradation in an osteoarthritic culture model. J Orthop Res 2005;23:118-126.

Hayashi K, Frank JD, Dubinsky C, et al. Histologic changes in ruptured canine cranial cruciate ligament. Vet Surg 2003;32:269-277.

Hayashi K, Frank JD, Hao Z, et al. Evaluation of ligament fibroblast viability in ruptured cranial cruciate ligament of dogs. Am J Vet Res 2003;64:1010-1016.

Hefti FL, Kress A, Fasel J, et al. Healing of the transected anterior cruciate ligament in the rabbit. J Bone Joint Surg Am 1991;73:373-383.

Hirokawa S, Yamamoto K, Kawada T. Circumferential measurement and analysis of strain distribution in the human ACL using a photoelastic coating method. J Biomech 2001;34:1135-1143.

Hollander JM, Martin JL, Belke DD, et al. Overexpression of wild-type heat shock protein 27 and a nonphosphorylatable heat shock protein 27 mutant protects against ischemia/reperfusion injury in a transgenic mouse model. Circulation 2004;110:3544-3552.

Hollister AM, Jatana S, Singh AK, et al. The axes of rotation of the stifle. Clin Orthop Relat Res 1993:259-268.

Horman S, Fokan D, Mosselmans R, et al. Anti-sense inhibition of small-heat-shock-protein (HSP27) expression in MCF-7 mammary-carcinoma cells induces their spontaneous acquisition of a secretory phenotype. Int J Cancer 1999;82:574-582.

Howard E. The Stifle In: Evans D, ed. Miller's Anatomy of the Dog. 3 ed. Philadelphia: Saunders, 1993;246.

Hummel KM, Petrow PK, Franz JK, et al. Cysteine proteinase cathepsin K mRNA is expressed in synovium of patients with rheumatoid arthritis and is detected at sites of synovial bone destruction. J Rheumatol 1998;25:1887-1894.

Ikeda N, Nozawa-Inoue K, Takagi R, et al. Development of the synovial membrane in the rat temporomandibular joint as demonstrated by immunocytochemistry for heat shock protein 25. Anat Rec A Discov Mol Cell Evol Biol 2004;279:623-635.

Iwaki H, Pinskerova V, Freeman MA. Tibiofemoral movement 1: the shapes and relative movements of the femur and tibia in the unloaded cadaver stifle. J Bone Joint Surg Br 2000;82:1189-1195.

Kanaya A, Deie M, Adachi N, et al. Intra-articular Injection of Mesenchymal Stromal Cells in Partially Torn Anterior Cruciate Ligaments in a Rat Model. Arthroscopy: The Journal of Arthroscopic & Related Surgery 2007;23:610-617.

Kitamura HP, Yanase H, Kitamura H, et al. Unique localization of protein gene product 9.5 in type B synoviocytes in the joints of the horse. J Histochem Cytochem 1999;47:343-352.

Klocke NW, Snyder PW, Widmer WR, et al. Detection of synovial macrophages in the joint capsule of dogs with naturally occurring rupture of the cranial cruciate ligament. Am J Vet Res 2005;66:493-499.

Kobayashi D, Kurosaka M, Yoshiya S, et al. Effect of basic fibroblast growth factor on the healing of defects in the canine anterior cruciate ligament. Stifle Surg Sports Traumatol Arthrosc 1997;5:189-194.

Kontny E, Chorazy-Massalska M, Rudnicka W, et al. Comparison of taurine chloramine and taurine bromamine effects on rheumatoid arthritis synoviocytes. Amino Acids 2007;32:447-452.

Krauspe R, Schmidt M, Schaible HG. Sensory innervation of the anterior cruciate ligament. An electrophysiological study of the response properties of single identified mechanoreceptors in the cat. J Bone Joint Surg Am 1992;74:390-397.

Kurosawa H, Walker PS, Abe S, et al. Geometry and motion of the stifle for implant and orthotic design. J Biomech 1985;18:487-499.

Lampman TJ, Lund, E.M., Lipowitz, A.J. Cranial cruciate disease: current status of diagnosis, surgery, and risk for disease. Vet Comp Orthop Traumatol 2003 2003;16:122–126.

Lawrence D, Bao S, Canfield PJ, et al. Elevation of immunoglobulin deposition in the synovial membrane of dogs with cranial cruciate ligament rupture. Vet Immunol Immunopathol 1998;65:89-96.

Lemburg AK, Meyer-Lindenberg, A., and Hewicker-Tratwein, M. Immunohistochemical characterization of inflammatory cell populations and adhesion molecule expression in synovial membranes from dogs with spontaneous cranial cruciate ligament rupture. Immunol Immunopathol 2004;97:231-240.

Liu SH, Al-Shaikh RA, Panossian V, et al. Estrogen affects the cellular metabolism of the anterior cruciate ligament. A potential explanation for female athletic injury. Am J Sports Med 1997;25:704-709.

Lopez MJ, Markel MD, Kalscheur V, et al. Hamstring graft technique for stabilization of canine cranial cruciate ligament deficient stifles. Vet Surg 2003;32:390-401.

Lopez MJ, Robinson SO, Quinn MM, et al. In vivo evaluation of intra-articular protection in a novel model of canine cranial cruciate ligament mid-substance elongation injury. Vet Surg 2006;35:711-720.

Maekawa K, Furukawa H, Kanazawa Y, et al. Electron and immunoelectron microscopy on healing process of the rat anterior cruciate ligament after partial transection: the roles of multipotent fibroblasts in the synovial tissue. Histol Histopathol 1996;11:607-619.

Masayoshi K, Higuchi, H., Kimura M., et al. Proprioception and performance after anterior cruciate ligament rupture. Int Orthop 2004;28:278-281.

Miron T, Vancompernolle K, Vandekerckhove J, et al. A 25-kD inhibitor of actin polymerization is a low molecular mass heat shock protein. J Cell Biol 1991;114:255-261.

Moore PF, Rossitto PV, Danilenko DM, et al. Monoclonal antibodies specific for canine CD4 and CD8 define functional T-lymphocyte subsets and high-density expression of CD4 by canine neutrophils. Tissue Antigens 1992;40:75-85.

Muir P, Hayashi K, Manley PA, et al. Evaluation of tartrate-resistant acid phosphatase and cathepsin K in ruptured cranial cruciate ligaments in dogs. Am J Vet Res 2002;63:1279-1284.

Mullan RH, Bresnihan B, Golden-Mason L, et al. Acute-phase serum amyloid A stimulation of angiogenesis, leukocyte recruitment, and matrix degradation in rheumatoid arthritis through an NF-kappaB-dependent signal transduction pathway. Arthritis Rheum 2006;54:105-114.

Murakami H, Shinomiya N, Kikuchi T, et al. Differential sensitivity to NO-induced apoptosis between anterior cruciate and medial collateral ligament cells. J Orthop Sci 2005;10:84-90.

Murakami H, Shinomiya N, Kikuchi T, et al. Upregulated expression of inducible nitric oxide synthase plays a key role in early apoptosis after anterior cruciate ligament injury. J Orthop Res 2006;24:1521-1534.

Murray MM, Martin, S.D., Martin T.L., et al. Histologic changes in human anterior cruciate ligament after rupture. J Bone Joint Surg Am 2000;82A:1387-1397.

Murray MM, Spindler KP, Devin C, et al. Use of a collagen-platelet rich plasma scaffold to stimulate healing of a central defect in the canine ACL. J Orthop Res 2006;24:820-830.

Murray MM, Weiler A, Spindler KP. Interspecies variation in the fibroblast distribution of the anterior cruciate ligament. Am J Sports Med 2004;32:1484-1491.

Nagai H, Miyamoto Y, Nakata A, et al. Isolation and characterization of synovial cells from the human temporomandibular joint. J Oral Pathol Med 2006;35:104-110.

Nawabi DH, Patel RV, Hall-Craggs M, et al. MRI-confirmed tear and spontaneous healing of the anterior cruciate ligament. Injury Extra 2006;37:125-128.

Niebauer GW, Menzel EJ. Immunological changes in canine cruciate ligament rupture. Res Vet Sci 1982;32:235-241.

Niebauer GW, Wolf B, Bashey RI, et al. Antibodies to canine collagen types I and II in dogs with spontaneous cruciate ligament rupture and osteoarthritis. Arthritis Rheum 1987;30:319-327.

Noyes FR, Mooar LA, Moorman CT, 3rd, et al. Partial tears of the anterior cruciate ligament. Progression to complete ligament deficiency. J Bone Joint Surg Br 1989;71:825-833.

O'Connor BL, Visco DM, Heck DA, et al. Gait alterations in dogs after transection of the anterior cruciate ligament. Arthritis Rheum 1989;32:1142-1147.

Oda A, Miyata M, Kodama E, et al. Antibodies to 65Kd heat-shock protein were elevated in rheumatoid arthritis. Clin Rheumatol 1994;13:261-264.

Odensten M, Gillquist J. Functional anatomy of the anterior cruciate ligament and a rationale for reconstruction. J Bone Joint Surg Am 1985;67:257-262.

Pavalko FM, LaRoche SM. Activation of human neutrophils induces an interaction between the integrin beta 2-subunit (CD18) and the actin binding protein alpha-actinin. J Immunol 1993;151:3795-3807.

Powers MY, Martinez SA, Lincoln JD, et al. Prevalence of cranial cruciate ligament rupture in a population of dogs with lameness previously attributed to hip dysplasia: 369 cases (1994-2003). J Am Vet Med Assoc 2005;227:1109-1111.

Qin X, Chua PK, Ohira RH, et al. An autocrine/paracrine role of human decidual relaxin. II. Stromelysin-1 (MMP-3) and tissue inhibitor of matrix metalloproteinase-1 (TIMP-1). Biol Reprod 1997;56:812-820.

Rifkin DB, Moscatelli D. Recent developments in the cell biology of basic fibroblast growth factor. J Cell Biol 1989;109:1-6.

Russinova A, Atanassova N, Kancheva L. Isolation and immunocytochemical characterization of a library of monoclonal antibodies directed against rat testicular antigens. Endocr Regul 2000;34:135-143.

Sakaguchi Y, Sekiya I, Yagishita K, et al. Comparison of human stem cells derived from various mesenchymal tissues: superiority of synovium as a cell source. Arthritis Rheum 2005;52:2521-2529.

Sathasivam S, Walker PS. A computer model with surface friction for the prediction of total stifle kinematics. J Biomech 1997;30:177-184.

Sharp P, Krishnan M, Pullar O, et al. Heat shock protein 27 rescues motor neurons following nerve injury and preserves muscle function. Exp Neurol 2006;198:511-518.

Shirasawa S, Sekiya I, Sakaguchi Y, et al. In vitro chondrogenesis of human synovium-derived mesenchymal stem cells: optimal condition and comparison with bone marrow-derived cells. J Cell Biochem 2006;97:84-97.

Singleton P. Nucleic Acid Amplification. DNA Methods in Clinical Microbiology. Dordrecht: Kluwer Academic Press, 2000;56-120.

Siu D, Rudan J, Wevers HW, et al. Femoral articular shape and geometry. A three-dimensional computerized analysis of the stifle. J Arthroplasty 1996;11:166-173.

Slauterbeck JR, Pankratz K, Xu KT, et al. Canine ovariohysterectomy and orchiectomy increases the prevalence of ACL injury. Clin Orthop Relat Res 2004:301-305.

Sledge CB, R. A., Walsh DA, Blake DR, DA Walsh, DR Blake Biology of the normal joint. Kelley's textbook of rheumatology In: S Ruddy CS, ed. Philadelphia: Saunders, 2001;1-24.

Slocum B, Slocum TD. Tibial plateau leveling osteotomy for repair of cranial cruciate ligament rupture in the canine. Vet Clin North Am Small Anim Pract 1993;23:777-795.

Smith PN, Refshauge KM, Scarvell JM. Development of the concepts of stifle kinematics. Arch Phys Med Rehabil 2003;84:1895-1902.

Sojka P, Sjolander P, Johansson H, et al. Influence from stretch-sensitive receptors in the collateral ligaments of the stifle joint on the gamma-muscle-spindle systems of flexor and extensor muscles. Neurosci Res 1991;11:55-62.

Spindler KP, Murray MM, Devin C, et al. The central ACL defect as a model for failure of intra-articular healing. J Orthop Res 2006;24:401-406.

Stevens CR, Mapp PI, Revell PA. A monoclonal antibody (Mab 67) marks type B synoviocytes. Rheumatol Int 1990;10:103-106.

Tifford CD, Jackson DW. Simultaneous bilateral anterior cruciate ligament ruptures in a cheerleader. Arthroscopy 2001;17:E17.

Vasanjee SC, Paulsen D, Hosgood G, et al. Characterization of normal canine anterior cruciate ligament-associated synoviocytes. J Orthop Res 2008.

Vasseur PB, Pool RR, Arnoczky SP, et al. Correlative biomechanical and histologic study of the cranial cruciate ligament in dogs. Am J Vet Res 1985;46:1842-1854.

Walker PS, Shoji H, Erkman MJ. The rotational axis of the stifle and its significance to prosthesis design. Clin Orthop Relat Res 1972;89:160-170.

Walsh DA, Sledge, C.B., and Blake, D.R. Biology of the Normal Joint In: Kelley WN, Ruddy, S., Harris, E.D., Sledge, C.B., ed. Textbook of Rheumatology. 5 ed. Philadelphia: W.B. Saunders, 1997;11-18.

Wickham MQ, Erickson GR, Gimble JM, et al. Multipotent stromal cells derived from the infrapatellar fat pad of the stifle. Clin Orthop Relat Res 2003:196-212.

Wilke VL, Kinghorn, B.P., Conzemius, M.G., et al. Prediction of inheritance for anterior cruciate ligament disease in the Newfoundland dog. ACVS Veterinary Symposium 2004.

Wilke VL, Robinson DA, Evans RB, et al. Estimate of the annual economic impact of treatment of cranial cruciate ligament injury in dogs in the United States. J Am Vet Med Assoc 2005;227:1604-1607.

Wilkinson LS, Pitsillides AA, Worrall JG, et al. Light microscopic characterization of the fibroblast-like synovial intimal cell (synoviocyte). Arthritis Rheum 1992;35:1179-1184.

Wingfield C, Amis AA, Stead AC, et al. Comparison of the biomechanical properties of rottweiler and racing greyhound cranial cruciate ligaments. J Small Anim Pract 2000;41:303-307.

Yanni G, Nabil M, Farahat MR, et al. Intramuscular gold decreases cytokine expression and macrophage numbers in the rheumatoid synovial membrane. Ann Rheum Dis 1994;53:315-322.

Yoshida M, Sai S, Marumo K, et al. Expression analysis of three isoforms of hyaluronan synthase and hyaluronidase in the synovium of stifles in osteoarthritis and rheumatoid arthritis by quantitative real-time reverse transcriptase polymerase chain reaction. Arthritis Res Ther 2004;6:R514-520.

Zhu P, Lu N, Shi ZG, et al. CD147 overexpression on synoviocytes in rheumatoid arthritis enhances matrix metalloproteinase production and invasiveness of synoviocytes. Arthritis Res Ther 2006;8:R44.

Zimny ML, Albright DJ, Dabezies E. Mechanoreceptors in the human medial meniscus. Acta Anat (Basel) 1988;133:35-40.

APPENDIX I: RAW DATA

Mean +/- SEM pixel number for each phenotype (Phen) at proximal (Prox), distal (Dist), middle (Mid), and central (Cent) regions of the normal canine CrCL.

Dog	Phen	Prox	Dist	Mid	Cent
270	HSP	406882	419155	388700	502688
270	CD18	442417	344719	90824	253628
270	DS	1299	96350	-	95051
271	HSP	27620	751881	681345	475263
271	CD18	220171	113770	81012	134283
271	DS	-	-	-	-
272	HSP	221114	284375	281368	316741
272	CD18	202332	276198	309215	436303
272	DS	7942	0	7498	5005
268	HSP	71318	85230	44457	78331
268	CD18	23242	27474	47057	23955
268	DS	-	333	-	-
269	HSP	180271	202831	243761	214367
269	CD18	114466	81857	48111	77150
269	DS	-	-	-	-
273	HSP	285866	209534	232314	202946
273	CD18	220286	139065	62237	1430998
273	DS	-	13230	38675	-
274	HSP	272721	433462	449109	461179
274	CD18	273653	178224	167811	359557
274	DS	-	-	-	-
265	HSP	65543	251205	241731	247545
265	CD18	29328	129592	32264	119274
265	DS	-	-	8062	-
266	HSP	179628	190731	311185	261103
266	CD18	44773	145173	62922	104427
266	DS	-	46450	-	14457
267	HSP	172288	156630	275538	236792
267	CD18	64903	53894	104687	138426
267	DS	2977	8094	3867	6797

Mean +/- SEM pixel number for each phenotype (Phen) at lateral (Lat), medial (Med), cranial (Cr), and caudal (Ca) regions of the normal canine CrCL.

Dog	Phen	Lat	Med	Cr	Ca
270	HSP	414024	298025	661408	553329
270	CD18	273724	350608	573984	303976
270	DS	-	2598	96350	1299
271	HSP	687113	547120	1017432	692064
271	CD18	129448	151222	317963	96990
271	DS	-	-	-	-
272	HSP	287068	183048	309904	476953
272	CD18	285938	65504	347754	439991
272	DS	7498	2937	2937	12503
268	HSP	122674	-	129626	272384
268	CD18	73818	-	72290	123256
268	DS	333	-	-	666
269	HSP	412496	-	323601	930125
269	CD18	167284	-	150664	338204
269	DS	-	-	-	-
273	HSP	348762	176006	443829	1012139
273	CD18	176699	101791	338782	504394
273	DS	51905	-	51905	51905
274	HSP	390745	303368	660650	494642
274	CD18	191957	68174	121928	497760
274	DS	-	-	-	-
265	HSP	110770	200164	954679	162279
265	CD18	50808	21102	265241	117127
265	DS	8062	-	16124	-
266	HSP	202851	217590	959163	403925
266	CD18	24083	124358	346965	158771
266	DS	30413	1580	76863	16037
267	HSP	231275	136389	402913	201543
267	CD18	63931	21127	90247	133237
267	DS	4274	3867	14938	-

APPENDIX II: COMPARISON OF NORMAL AND ABNORMAL CRCLs

Pixel percentage for each phenotype at distal (D), middle (Mi), proximal (P), lateral (L), and medial regions of control CrCLs.

Dog	Phen	Region	Percentage
3438	HSP	DL	97.45254
3438	CD18	DL	2.54746
3438	DS	DL	0
3438	HSP	DM	100
3438	CD18	DM	0
3438	DS	DM	0
3438	HSP	MiL	74.37
3438	CD18	MiL	16.48
3438	DS	MiL	9.15
3438	HSP	MiM	100
3438	CD18	MiM	0
3438	DS	MiM	0
3438	HSP	PL	100
3438	CD18	PL	0
3438	DS	PL	0
3438	HSP	PM	96.75
3438	CD18	PM	0
3438	DS	PM	3.25
3951	HSP	DL	86.58
3951	CD18	DL	12.42
3951	DS	DL	1
3951	HSP	DM	64.25
3951	CD18	DM	27.66
3951	DS	DM	8.09
3951	HSP	MiL	14.48
3951	CD18	MiL	74.89
3951	DS	MiL	10.62
3951	HSP	MiM	100
3951	CD18	MiM	0
3951	DS	MiM	0
3951	HSP	PL	89.24
3951	CD18	PL	3.29
3951	DS	PL	7.47
3951	HSP	PM	13.5
3951	CD18	PM	85.49
3951	DS	PM	1
4611	HSP	DL	100
4611	CD18	DL	0
4611	DS	DL	0

4611	HSP	DM	40.88
4611	CD18	DM	0
4611	DS	DM	59.12
4611	HSP	MiL	100
4611	CD18	MiL	0
4611	DS	MiL	0
4611	HSP	MiM	19.98
4611	CD18	MiM	80.01
4611	DS	MiM	0.09
4611	HSP	PL	31.43
4611	CD18	PL	14
4611	DS	PL	54.56
4611	HSP	PM	89.17
4611	CD18	PM	0
4611	DS	PM	10.82
3115	HSP	DL	100
3115	CD18	DL	0
3115	DS	DL	0
3115	HSP	DM	98.77
3115	CD18	DM	0
3115	DS	DM	1.23
3115	HSP	MiL	100
3115	CD18	MiL	0
3115	DS	MiL	0
3115	HSP	MiM	100
3115	CD18	MiM	0
3115	DS	MiM	0
3115	HSP	PL	0
3115	CD18	PL	-
3115	DS	PL	-
3115	HSP	PM	-
3115	CD18	PM	-
3115	DS	PM	-

Pixel percentage for each phenotype at distal (D), middle (Mi), proximal (P), lateral (L), and medial regions of artificially stretched CrCLs.

Dog	Phen	Region	Percentage
3438LDL	HSP	3438LDL	91.91
3438LDL	CD18	3438LDL	6.55
3438LDL	DS	3438LDL	1.54
3438LDM	HSP	3438LDM	99.8
3438LDM	CD18	3438LDM	0.2
3438LDM	DS	3438LDM	0
3438LMiL	HSP	3438LMiL	94.37
3438LMiL	CD18	3438LMiL	4.63
3438LMiL	DS	3438LMiL	1
3438LMiM	HSP	3438LMiM	97.59
3438LMiM	CD18	3438LMiM	1.45
3438LMiM	DS	3438LMiM	0.96
3438LPLF	HSP	3438LPLF	96.07
3438LPLF	CD18	3438LPLF	1.16
3438LPLF	DS	3438LPLF	2.77
3438LPM	HSP	3438LPM	92.26
3438LPM	CD18	3438LPM	0.79
3438LPM	DS	3438LPM	6.96
3579RDL	HSP	3579RDL	87.7
3579RDL	CD18	3579RDL	3.31
3579RDL	DS	3579RDL	8.98
3579RDM	HSP	3579RDM	86.97
3579RDM	CD18	3579RDM	12.38
3579RDM	DS	3579RDM	0.66
3579RMiL	HSP	3579RMiL	100
3579RMiL	CD18	3579RMiL	0
3579RMiL	DS	3579RMiL	0
3579RMiM	HSP	3579RMiM	100
3579RMiM	CD18	3579RMiM	0
3579RMiM	DS	3579RMiM	0
3579RPL	HSP	3579RPL	0.61
3579RPL	CD18	3579RPL	98.3
3579RPL	DS	3579RPL	1.13
3579RPM	HSP	3579RPM	65.47
3579RPM	CD18	3579RPM	4.27
3579RPM	DS	3579RPM	30.26
3951RDL	HSP	3951RDL	98
3951RDL	CD18	3951RDL	0
3951RDL	DS	3951RDL	1.97
3951RDM	HSP	3951RDM	100
3951RDM	CD18	3951RDM	0

3951RDM	DS	3951RDM	0
3951RMiL	HSP	3951RMiL	100
3951RMiL	CD18	3951RMiL	0
3951RMiL	DS	3951RMiL	0
3951RMiM	HSP	3951RMiM	100
3951RMiM	CD18	3951RMiM	0
3951RMiM	DS	3951RMiM	0
3951RPL	HSP	3951RPL	-
3951RPL	CD18	3951RPL	-
3951RPL	DS	3951RPL	-
3951RPM	HSP	3951RPM	35.11
3951RPM	CD18	3951RPM	57.37
3951RPM	DS	3951RPM	7.52
3471RDL		3471RDL	-
3471RDL		3471RDL	-
3471RDL		3471RDL	-
3471RDM		3471RDM	-
3471RDM		3471RDM	-
3471RDM		3471RDM	-
3471RMiL	HSP	3471RMiL	57.68
3471RMiL	CD18	3471RMiL	40.76
3471RMiL	DS	3471RMiL	1.56
3471RMiM		3471RMiM	-
3471RMiM		3471RMiM	-
3471RMiM		3471RMiM	-
3471RPL	HSP	3471RPL	78.7
3471RPL	CD18	3471RPL	13.97
3471RPL	DS	3471RPL	7.33
3471RPM		3471RPM	-
3471RPM		3471RPM	-
3471RPM		3471RPM	-
3732LDL	HSP	3732LDL	100
3732LDL	CD18	3732LDL	0
3732LDL	DS	3732LDL	0
3732LDM	HSP	3732LDM	21.35
3732LDM	CD18	3732LDM	69.03
3732LDM	DS	3732LDM	9.61
3732LMiL	HSP	3732LMiL	100
3732LMiL	CD18	3732LMiL	0
3732LMiL	DS	3732LMiL	0
3732LMiM	HSP	3732LMiM	100
3732LMiM	CD18	3732LMiM	0
3732LMiM	DS	3732LMiM	0
3732LPL	HSP	3732LPL	99.9
3732LPL	CD18	3732LPL	0

3732LPL	DS	3732LPL	0.1
3732LPM	HSP	3732LPM	99.86
3732LPM	CD18	3732LPM	0.14
3732LPM	DS	3732LPM	0
3115LDL	HSP	3115LDL	-
3115LDL	CD18	3115LDL	-
3115LDL	DS	3115LDL	-
3115LDM	HSP	3115LDM	100
3115LDM	CD18	3115LDM	0
3115LDM	DS	3115LDM	0
3115LMiL	HSP	3115LMiL	100
3115LMiL	CD18	3115LMiL	0
3115LMiL	DS	3115LMiL	0
3115LMiM	HSP	3115LMiM	100
3115LMiM	CD18	3115LMiM	0
3115LMiM	DS	3115LMiM	0
3115LPL	HSP	3115LPL	87.12
3115LPL	CD18	3115LPL	0
3115LPL	DS	3115LPL	12.88
3115LPM	HSP	3115LPM	73.2
3115LPM	CD18	3115LPM	20.66
3115LPM	DS	3115LPM	6.13
4611LDL	HSP	4611LDL	99.88
4611LDL	CD18	4611LDL	0.03
4611LDL	DS	4611LDL	0.09
4611LDM	HSP	4611LDM	100
4611LDM	CD18	4611LDM	0
4611LDM	DS	4611LDM	0
4611LMiL	HSP	4611LMiL	-
4611LMiL	CD18	4611LMiL	-
4611LMiL	DS	4611LMiL	-
4611LMiM	HSP	4611LMiM	99.51
4611LMiM	CD18	4611LMiM	0
4611LMiM	DS	4611LMiM	0.49
4611LPL	HSP	4611LPL	83.91
4611LPL	CD18	4611LPL	1.94
4611LPL	DS	4611LPL	14.14
4611LPM	HSP	4611LPM	100
4611LPM	CD18	4611LPM	0
4611LPM	DS	4611LPM	0
4712LDL	HSP	4712LDL	69.18
4712LDL	CD18	4712LDL	0.61
4712LDL	DS	4712LDL	30.21
4712LDM	HSP	4712LDM	60.66
4712LDM	CD18	4712LDM	10.46

4712LDM	DS	4712LDM	28.88
4712LMiL	HSP	4712LMiL	88.37
4712LMiL	CD18	4712LMiL	0
4712LMiL	DS	4712LMiL	11.63
4712LMiM	HSP	4712LMiM	60.06
4712LMiM	CD18	4712LMiM	0
4712LMiM	DS	4712LMiM	39.94
4712LPL	HSP	4712LPL	79.17
4712LPL	CD18	4712LPL	0
4712LPL	DS	4712LPL	20.83
4712LPM	HSP	4712LPM	69.57
4712LPM	CD18	4712LPM	0.84
4712LPM	DS	4712LPM	29.6

Pixel percentage for each phenotype at distal (D), middle (Mi), proximal (P), lateral (L), and medial regions of partially disrupted CrCLs.

Dog	Phen	Region	Percentage
3732	HSP	DL	-
3732	CD18	DL	-
3732	DS	DL	-
3732	HSP	DM	-
3732	CD18	DM	-
3732	DS	DM	-
3732	HSP	MiL	100
3732	CD18	MiL	0
3732	DS	MiL	0
3732	HSP	MiM	80.52
3732	CD18	MiM	4.47
3732	DS	MiM	15
3732	HSP	PL	93.02
3732	CD18	PL	4.33
3732	DS	PL	2.64
3732	HSP	PM	100
3732	CD18	PM	0
3732	DS	PM	0
3471	HSP	DL	100
3471	CD18	DL	0
3471	DS	DL	0
3471	HSP	DM	100
3471	CD18	DM	0
3471	DS	DM	0
3471	HSP	MiL	98.08
3471	CD18	MiL	0
3471	DS	MiL	1.92
3471	HSP	MiM	100
3471	CD18	MiM	0
3471	DS	MiM	0
3471	HSP	PL	32
3471	CD18	PL	64.15
3471	DS	PL	3.84
3471	HSP	PM	54.68
3471	CD18	PM	44.94
3471	DS	PM	0.38
4712	HSP	DL	93.12
4712	CD18	DL	0
4712	DS	DL	6.88
4712	HSP	DM	95.63
4712	CD18	DM	0

4712	DS	DM	4.37
4712	HSP	MiL	-
4712	CD18	MiL	-
4712	DS	MiL	-
4712	HSP	MiM	-
4712	CD18	MiM	-
4712	DS	MiM	-
4712	HSP	PL	-
4712	CD18	PL	-
4712	DS	PL	-
4712	HSP	PM	-
4712	CD18	PM	-
4712	DS	PM	-
3476	HSP	DL	34.96
3476	CD18	DL	28.07
3476	DS	DL	36.97
3476	HSP	DM	93.09
3476	CD18	DM	0.68
3476	DS	DM	6.23
3476	HSP	MiL	66.41
3476	CD18	MiL	0.1
3476	DS	MiL	33.49
3476	HSP	MiM	92.91
3476	CD18	MiM	1.3
3476	DS	MiM	5.78
3476	HSP	PL	92.49
3476	CD18	PL	5.8
3476	DS	PL	1.7
3476	HSP	PM	57.06
3476	CD18	PM	40.61
3476	DS	PM	2.33

APPENDIX III: LETTER OF PERMISSION FROM THE JOURNAL OF ORTHOPEDIC RESEARCH

April 3 2008

Sunil C. Vasanjee
LSU School of Veterinary Medicine
Skip Bertman Dr
Baton Rouge, LA 70803

Dear Mr Vasanjee

The *Journal of Orthopedic Research* grants you permission to include the manuscript entitled "Characterization of normal canine anterior cruciate ligament associated synoviocytes" as a chapter in your thesis to fulfill requirements of your MS program.

Sincerely,

Timothy M. Wright, PhD
Co-Editor

VITA

Sunil Vasanjee was born in Bulawayo, Zimbabwe. He completed a Bachelor of Veterinary Science Degree at the University of Zimbabwe in 2000. He went on to work in private practice for 2 years. From August 2002 to July 2003 he completed a surgical fellowship at Louisiana State University in Baton Rouge, Louisiana. He then completed a rotating companion animal medicine and surgery internship at Louisiana State University between July 2003 and July 2004. The following year, from July 2004 to July 2005 he completed a comparative orthopedic research fellowship at Louisiana State University. In July 2005 he started a residency in companion animal surgery at Louisiana State University. In August 2005 he was admitted into the graduate school at Louisiana State University. He will be awarded the degree of Master of Science in veterinary medical sciences in May 2008 and he will complete his residency in July 2008.